Supplement to "Exploring the sensitivity of atmospheric nitrate concentrations to nitric acid uptake rate using the Met Office's Unified Model" by A.C. Jones *et al.*

S1 Primary Ammonium Nitrate Production

S1.1 Determine the equilibration constant (K_p) of the ammonium-nitrate system

Free ammonia is used for the neutralization of nitric acid to ammonium nitrate aerosol following the equilibrium reaction:

$$\mathrm{HNO_3} + \mathrm{NH_3} \leftrightarrow \mathrm{NH_4 \cdot NO_3} \quad [S1]$$

The equilibrium constant (K_p) of (1) strongly depends on relative humidity and temperature. The parameterization used for this dependence is based on Mozurkewich (1993). First, the deliquescence relative humidity (*DRH*, %) is calculated based on Seinfeld and Pandis (1998):

$$DRH = \exp\left(\frac{723.7}{T} + 1.6954\right) \quad [S2]$$

where T is the air temperature (K). For relative humidities lower than DRH, $K_p = K_{pd}$ and is calculated with:

$$K_{pd} = \exp\left[118.87 - \frac{24084}{T} - 6.025\ln(T)\right] \quad [S3]$$

For relative humidities higher than DRH, $K_p = K_{ph}$ and depends on both temperature and relative humidity (*RH*, %) and is calculated based on:

$$K_{ph} = K_{pd}\left(p_1 - p_2 RH_1 + p_3 {RH_1}^2\right){RH_1}^{1.75} \quad [S4]$$

With RH_1 defined as (1-*RH*/100) and p_1, p_2, and p_3 provided by:

$$p_1 = \exp\left[-135.94 + \frac{8763}{T} + 19.12\ln(T)\right] \quad [S5a]$$

$$p_2 = \exp\left[-122.65 + \frac{9969}{T} + 16.22\ln(T)\right] \quad [S5b]$$

$$p_3 = \exp\left[-182.61 + \frac{13875}{T} + 24.46\ln(T)\right] \quad [S5c]$$

S1.2 Determine the equilibration time scale (τ) for the ammonium-nitrate system

Ammonium nitrate formation is a condensation process rather than nucleation process (Ackerman *et al.*, 1995) and therefore depends on the concentration and properties of existing atmospheric aerosol. In UKCA-mode, each lognormal mode is represented by an overall particle number mixing ratio (*N* in

eq-kg/kg(air)) and individual constituent mass mixing ratios (*M* in kg/kg(air)). Each constituent (e.g. dust, sulphate, etc) is associated with a density (ρ) and molar mixing ratio. Each mode has its own fixed width parameter (σ). The geometric median diameter for the mode (D_p) can be calculated thus:

$$D_{p,r} = \left[\frac{6}{\pi \, e^{4.5 \ln^2 \sigma_r}} \times \frac{k_B}{R} \times \frac{1}{N_r} \sum_x \frac{M_{x,r}}{\rho_x} \right]^{1/3} \qquad [S6]$$

The indices *r* and *x* represent the mode and constituent respectively. $R = 287.05$ J Kg^{-1} K^{-1} is the specific gas constant of dry air and $k_B = 1.3804 \times 10^{-23}$ J K^{-1} is the Boltzmann constant. Using properties of the lognormal distribution, the modal mean diameter D_μ is then:

$$D_{\mu,r} = D_{p,r} \, e^{0.5 \ln^2 \sigma_r} \qquad [S7]$$

UKCA-mode explicitly calculates hygroscopic growth using the Zdanovskii-Stokes-Robinson (ZSR) algorithm, with aerosol-associated water volume a diagnostic rather than a prognostic. As the UKCA emissions scheme precedes UKCA-mode within the UKCA calling sequence, the water content and concomitantly the hygroscopic growth factor is not readily available to the nitrate production scheme. Instead we grow the particles using a relative humidity dependent growth parameterisation based on ammonium sulphate (Gerber *et al.*, 1985).

$$D_{w,r} = 2 \times \left[\frac{0.6628 \, {D_{\mu,r}}^{3.082}}{1.1658 \times 10^{-13} \, {D_{\mu,r}}^{-1.428} - \log_{10} \frac{RH}{100}} + {D_{\mu,r}}^3 \right]^{1/3} \qquad [S8]$$

To test the Gerber parameterisation, we utilise annual-mean climatology from an atmosphere-only integration of the MetUM (N96). Annual-mean aerosol wet diameters from UKCA for aerosol mode (calculated using the ZSR scheme every time-step) are compared to wet diameters from applying the Gerber parameterisation to annual-mean dry diameters. Every grid-cell below the tropopause (i.e. the bottom-most 49 levels) is treated equally irrespective of aerosol number concentration and the results presented for Aitken and accumulation modes in Figure S1. The Gerber parameterisation over-estimates hygroscopic growth compared to ZSR for many gridcells in which the actual diameter > 0.25 μm owing probably to the differing aerosol compositions which is not accounted for in Eq. S8.

We follow Makar *et al*. (1998) in expressing the equilibration time scale (τ) as the reciprocal of the product of a condensation rate (k_{HNO3}) and the number concentration of aerosol particles (*N*). The Schwartz (1986) first-order uptake scheme is utilised to determine k_{HNO3} for each mode (Eqs S9-S12).

$$D_g = \frac{3}{8 A_c \rho_a d_a^2} \left[\frac{m_a R_a T}{2\pi} \times \frac{m_a + m_{HNO3}}{m_{HNO3}} \right]^{\frac{1}{2}} \qquad [S9]$$

$$\lambda = \frac{3D_g}{\upsilon} = \frac{3D_g}{\sqrt{\frac{8R_aT}{\pi m_{HNO3}}}} \quad [S10]$$

$$K_{n,r} = \frac{2\lambda}{D_{w,r}} \quad [S11]$$

$$k_{HNO3,r} = \frac{2\pi D_{w,r} D_g}{1 + \frac{4K_{n,r}}{3\gamma} \times \left(1 - \frac{0.47\gamma}{1 + K_{n,r}}\right)} \quad [S12]$$

Equations S9-S12 determine the molecular diffusivity coefficient (D_g, m^2s^{-1}), the mean free path (λ, m), the Knudsen number (K_n), and the modal condensation rate ($k_{HNO3,r}$, m^3s^{-1}). Constants in the algorithm include the Avogadro constant $A_c = 6.022 \times 10^{23}$ mol^{-1}, the gas constant of dry air $R_a = 8.314$ J mol^{-1} K^{-1}, the molar mass of dry air $m_a = 0.029$ kg mol^{-1}, the molar mass of HNO_3 $m_{HNO3} = 0.063$ kg mol^{-1}, the molecular diameter of dry air $d_a = 4.5 \times 10^{-10}$m, and the reactive uptake coefficient (γ) for HNO_3 which we assume to be invariant at 0.193 (Feng and Penner, 2007). Variables in Eqs S9-S12 include the temperature T (K) and air density ρ_a (kg m^{-3}). In Eq S10, υ is the mean molecular speed (m s^{-1}).

Equations S9-S12 are also applied to CLASSIC dust bins 1-3 (Woodward *et al*., 2001), with representative diameters ($D_{w,r}$ in Eqs S11 and S12) of 0.088 μm, 0.28 μm and 0.88 μm for Bins 1-3 respectively. The RH-dependent uptake coefficient for dust (γ) follows Fairlie *et al.* (2010). Finally, multiplying the rate coefficients (*k)* by particle number concentrations (*N*, m^{-3}) gives the rate at which HNO_3 gas is transferred to the aerosol phase (*Nk*, s^{-1}).

$$Nk_{AIT} = k_{HNO3,ait} \times N_{ait} + k_{dust,bin1} \times N_{dust,bin1} \quad [S13]$$

$$Nk_{ACC} = k_{HNO3,acc} \times N_{acc} + k_{dust,bin2} \times N_{dust,bin2} + 0.5 \times k_{dust,bin3} \times N_{dust,bin3} \quad [S14]$$

The equilibrium timescale (τ) is then:

$$\tau = \frac{1}{Nk_{AIT} + Nk_{ACC}} \quad [S15]$$

The same annual-mean fields as utilised for the Gerber approximation (Fig.S1) are used to investigate the equilibrium timescale (Fig. S3) and the accumulation to Aitken production ratio (Fig.S4). Over key ammonium nitrate regions such as Europe, South East Asia and Eastern North America, the equilibrium timescale is less than 10 minutes up to a nominal altitude of 2 km (Fig. S3). This is commensurate with the typical timescales in Ackerman *et al.* (1995) for particles with radii between 0.1 and 0.5 μm. At the surface, ammonium nitrate production is, on a global-mean basis, a factor of 8 greater than Aitken production, which reduces to a factor of 1.5 at 3 km altitude owing to the preponderance of smaller aerosols at higher altitudes (Fig. S4).

S1.3 Determine the ammonium sulphate neutralization state

Mass mixing ratios from UKCA $[X]$ are firstly converted to molar concentrations $\{X\} = \frac{[X]\rho_a}{M_X}$, where ρ_a is the air density in (kg m^{-3}) and M_X is the molar weight of substance *X* in (kg mol-1).Modal concentrations are denoted by $\{X\}_r$ where the subscript $r = 1, \ldots, 3$ denotes the mode (Aitken, accumulation and coarse respectively). Total concentrations are denoted by $\{X\}$ where $\{X\} = \sum_{r=1,3}\{X\}_r$. Output quantities are denoted $\{\dot{X}\}$.

Total ammonia, nitrate and sulphate molar concentrations use a different notation, following Hauglustaine *et al*. (2014).

$$T_N = \{NO_3\} + \{HNO_3\} \quad [S16a]$$

$$T_A = \{NH_4\} + \{NH_3\} \quad [S16b]$$

$$T_S = \{SO_4\} \quad [S16c]$$

The sulphate equilibrium state is determined using the concentrations of ammonia (T_A) and sulphate (T_S) following Metzger *et al*. (2002):

$$\Gamma_{SO_4} = \begin{cases} 2 & 2\,T_S < T_A & 2NH_3 + H_2SO_4 \rightarrow (NH_4)_2SO_4 \\ 1.5 & T_S < T_A < 2\,T_S & 3NH_3 + 2H_2SO_4 \rightarrow (NH_4)_3H(SO_4)_2 \\ 1 & T_A < T_S & NH_3 + H_2SO_4 \rightarrow (NH_4)HSO_4 \end{cases} \quad [S17a]$$

The total number of moles of ammonia that remain after SO_4 neutralization equals:

$$T_A^* = \text{Max}\,(0\,, T_A - \Gamma_{SO_4} \times T_S) \quad [S18]$$

However, the aim is to neutralise SO_4 mode by mode (starting with the smallest mode) to determine the existing NH4 mixing ratio associated with SO_4, which is achieved using the following algorithm:

Initial conditions (total available ammonia + ammonium for neutralisation):

$$T_{A,\text{rem}} = T_A \quad [S19a]$$

For $r = 1, \ldots, 3$ where r denotes the size mode (1=Aitken, 2=Accumulation, 3=Coarse), the moles of NH_4 associated with existing SO_4 equals:

$$\{NH_4(\dot{SO}_4)\}_r = \text{Min}\left(T_{A,\text{rem}}\,, \Gamma_{SO_4} \times \{SO_4\}_r\right) \quad [S19b]$$

$$T_{A,\text{rem}} = \text{Max}\left(0, T_{A,\text{rem}} - \{NH_4(\dot{SO}_4)\}_r\right) \quad [S19c]$$

It can be shown that:

$$T_A^* = \text{Max}\left(0\,, T_A - \Gamma_{SO_4} \times T_S\right) \equiv \text{Max}\left(0\,, T_A - \sum_{r=1,3}\{NH_4(\dot{SO}_4)\}_r\right) \quad [S20]$$

The overlying dot in $\{\mathrm{NH_4}(\dot{\mathrm{SO_4}})\}_r$ is to differentiate output quantities from input. Also, let $\{\mathrm{NH_4}(\dot{\mathrm{SO_4}})\} = \sum_{r=1,3}\{\mathrm{NH_4}(\dot{\mathrm{SO_4}})\}_i$ denote the total $\mathrm{NH_4}$ concentration associated with sulphate. The next step will also require the concentration of NH_3 gas used to neutralise SO_4:

$$\{\mathrm{NH_3}(\dot{\mathrm{SO_4}})\} = \mathrm{Max}\left(0, \{\mathrm{NH_4}(\dot{\mathrm{SO_4}})\} - \{\mathrm{NH_4}\}\right) \quad [S21]$$

S1.4 Produce ammonium nitrate if enough ammonium remains

If $T_A^* T_N > K_p$, then ammonium nitrate forms from the condensation of ammonia and nitric acid onto existing aerosol particles. Firstly, the number of moles of $\{\mathrm{NH_4}\dot{\mathrm{NO_3}}\}$ in equilibrium is calculated according to Seinfeld and Pandis (1998):

$$\{\mathrm{NH_4}\dot{\mathrm{NO_3}}\} = \frac{1}{2}\left[T_A^* + T_N - \sqrt{(T_A^* + T_N)^2 - 4\left(T_N T_A^* - K_p\right)}\right] \quad [S22]$$

Before calculating the time-dependent concentration of ammonium nitrate, it is first necessary to update the NH_3 concentration for any neutralisation of SO_4 that might have occurred:

$$\{\mathrm{NH_3}\}_u = \mathrm{Max}\left(0, \{\mathrm{NH_3}\} - \{\mathrm{NH_3}(\dot{\mathrm{SO_4}})\}\right) \quad [S23]$$

The equilibrium concentrations of HNO_3 and NH_3 are calculated thus:

$$\{\mathrm{NH_3}\}_{eq} = \mathrm{Max}\left(0, T_A^* - \{\mathrm{NH_4}\dot{\mathrm{NO_3}}\}\right) \quad [S24a]$$

$$\{\mathrm{HNO_3}\}_{eq} = \mathrm{Max}\left(0, T_N - \{\mathrm{NH_4}\dot{\mathrm{NO_3}}\}\right) \quad [S24b]$$

The equilibrium timescale (τ) from Section S1.2 (Eq. S15) is now introduced. The time-dependent concentrations of HNO_3 and NH_3 (accounting for the model time-step Δt) are now calculated:

$$\{\dot{\mathrm{NH_3}}\} = \mathrm{Max}\left(0, \{\mathrm{NH_3}\}_u - \left(1 - e^{-\frac{\Delta t}{\tau}}\right) \times \left(\{\mathrm{NH_3}\}_u - \{\mathrm{NH_3}\}_{eq}\right)\right) \quad [S25a]$$

$$\{\dot{\mathrm{HNO_3}}\} = \mathrm{Max}\left(0, \{\mathrm{HNO_3}\} - \left(1 - e^{-\frac{\Delta t}{\tau}}\right) \times \left(\{\mathrm{HNO_3}\} - \{\mathrm{HNO_3}\}_{eq}\right)\right) \quad [S25b]$$

The time-dependent total molar concentrations of NO_3 and HNO_3 are re-calculated:

$$\{\dot{\mathrm{NH_4}}\} = \mathrm{Max}\left(0, T_A^* - \{\dot{\mathrm{NH_3}}\}\right) \quad [S26a]$$

$$\{\dot{\mathrm{NO_3}}\} = \mathrm{Max}\left(0, T_N - \{\dot{\mathrm{HNO_3}}\}\right) \quad [S26b]$$

The quantities in Eq S26 represent total molar concentrations. In order to speciate the concentration between modes, the following algorithm (Eq S27) is utilised. Note that the variables N_r and k_r in Eq 27b are the modal number concentrations and uptake coefficients from Section S1.2 (Eqs S13 and S14) where $N_r = k_r = 0$ for $r = 3$ (the coarse mode).

Initial conditions (NH_4 available for NO_3 association):

$$T_{\mathrm{NH_4,rem}} = \{\dot{\mathrm{NH}}_4\} \quad [S27a]$$

For $r = 1, \ldots, 3$ where r denotes the size mode (1=Aitken, 2=Accumulation, 3=Coarse), the moles of NH_4 associated with existing NO_3 equals:

$$\frac{\Delta\{\mathrm{NO_3}\}_r}{\Delta t} = \frac{\left(\{\dot{\mathrm{NO}}_3\} - \{\mathrm{NO_3}\}\right)}{\Delta t} \times \frac{N_r k_r}{\sum_r N_r k_r} \quad [S27b]$$

$$\{\mathrm{NH_4}(\dot{\mathrm{NO}}_3)\}_r = \mathrm{Min}\left(T_{\mathrm{NH_4,rem}}, \{\mathrm{NO_3}\}_r + \frac{\Delta\{\mathrm{NO_3}\}_r}{\Delta t} \times \Delta t\right) \quad [S27c]$$

$$T_{\mathrm{NH_4,rem}} = \mathrm{Max}\left(0, T_{\mathrm{NH_4,rem}} - \{\mathrm{NH_4}(\dot{\mathrm{NO}}_3)\}_r\right) \quad [S27d]$$

Any remaining NH_4 (i.e. $T_{\mathrm{NH_4,rem}} > 0$) is added to the Aitken mode.

S1.5 Disassociate existing ammonium nitrate if $T_A^* T_N \leq K_p$

In low concentrations of ammonia and nitrate, any existing ammonium nitrate aerosol disassociates, i.e. for modes $r = 1, \ldots, 3$:

$$\frac{\Delta\{\mathrm{NO_3}\}_r}{\Delta t} = -\frac{\{\mathrm{NO_3}\}_r}{\Delta t} \quad [S28]$$

$$\{\mathrm{NH_4}(\dot{\mathrm{NO}}_3)\}_r = 0 \quad [S29]$$

S1.6 Calculate ammonium, ammonia and nitric acid tendencies

The ammonium tendency is the difference between the accumulated ammonium associated with sulphate and nitrate (as diagnosed above) and the input concentration of ammonium (Eq. S30). The nitric acid and ammonia tendencies are determined from the total nitrate and ammonium tendencies respectively (Eqs S31 and S32). All tendencies are the inverted to mass mixing ratios using $[X] = \frac{\{X\}M_X}{\rho_a}$ where M_X is the molar weight of substance X and ρ_a is the air density.

$$\frac{\Delta\{\mathrm{NH_4}\}_r}{\Delta t} = \frac{\{\mathrm{NH_4}(\dot{\mathrm{NO}}_3)\}_r + \{\mathrm{NH_4}(\dot{\mathrm{SO}}_4)\}_r - \{\mathrm{NH_4}\}_r}{\Delta t} \quad [S30]$$

$$\frac{\Delta\{\mathrm{HNO_3}\}}{\Delta t} = -\sum_r \frac{\Delta\{\mathrm{NO_3}\}_r}{\Delta t} \quad [S31]$$

$$\frac{\Delta\{\mathrm{NH_3}\}}{\Delta t} = -\sum_r \frac{\Delta\{\mathrm{NH_4}\}_r}{\Delta t} \quad [S32]$$

Checks are then made to ensure that HNO_3 and NH_3 mass concentrations are not less than zero at the end of the timestep and that number is also removed if, by dissociation (Section S1.4), total aerosol mass in a mode is zeroed. NH_3 and HNO_3 concentrations are updated at the end of the module.

S2 Coarse mode nitrate production

Nitric acid irreversibly condenses onto dust and sea-salt particles to form calcium nitrate and sodium nitrate respectively (Wang and Laskin, 2014). This reaction is slower than ammonium nitrate production, therefore numerically ammonium nitrate production is solved first. In the new UKCA-mode nitrate scheme, coarse nitrate is present in the accumulation and coarse soluble modes. Although functionality has been added for NO_3 uptake on CLASSIC 2 bin dust and the UKCA 2 insoluble mode dust scheme, only the CLASSIC 6-bin dust scheme (default in the N96 configuration at the time of writing) is described here.

S2.1 Calculate sea-salt number concentration and modal diameter

For every gridcell, the scheme first determines the dry median diameter ($D_{SS,r}$) for the accumulation and coarse soluble modes using Eq. S6 and then, under the assumption that sea-salt is externally mixed, the number concentration of sea-salt particles ($N_{SS,r}$ in m^{-3}) using the sea-salt mass mixing ratio ($M_{SS,r}$), modal width (σ_r), sea-salt density (ρ_{SS}), and air density (ρ_a):

$$N_{SS,r} = \frac{M_{SS,r}\rho_a}{\rho_{SS}\frac{\pi {D_{SS,r}}^3}{6}\, e^{4.5\ln^2\sigma_r}} \qquad [S33]$$

S2.2 Calculate dust number concentration

The CLASSIC dust scheme utilises 6 size bins with mass logarithmically spaced with diameter. Only nitrate condensing on bins 2-6 (i.e. accumulation and coarse modes) is considered by the scheme. The volume median diameters ($D_{du,b}$ where index $b = 2, \ldots, 6$ represents the bin) are 0.306, 0.966, 3.06, 9.66, and 30.6 μm. The dust number concentration per bin ($N_{du,b}$ in m^{-3}) is then determined from the dust mass mixing ratio ($M_{du,b}$), dust density (ρ_{du}), and air density (ρ_a):

$$N_{du,b} = \frac{M_{du,b}\rho_a}{\rho_{du}\frac{\pi {D_{du,b}}^3}{6}} \qquad [S34]$$

S2.3 Determine the RH-dependent reactive uptake coefficient for dust and sea-salt

The reactive uptake coefficients for dust (γ_{du}) and sea-salt (γ_{SS}) are linearly interpolated from observationally constrained values with relative humidity [Fairlie *et al*., 2010]. For the relative humidity values [15%, 30%, 70%, 80%], the γ_{du} values are [1×10^{-5}, 1×10^{-4}, 6×10^{-4}, 1.05×10^{-3}] and the γ_{SS} values are a factor of 100 greater at [1×10^{-3}, 1×10^{-2}, 6×10^{-2}, 1.05×10^{-1}], with no extrapolation at RH extrema (e.g. for RH > 80%, γ(RH=80%) is used).

S2.4 Determine the condensation rates for each sea-salt mode and dust bin

The first-order reactive uptake approximation (Fuchs and Sutugin, 1970; Schwartz, 1986) is used to determine condensation rates for each sea-salt mode and dust bin. The variables and constants are described in Section S1.2 (Eqs S9-S12) and the formulae again provided below.

$$D_g = \frac{3}{8A_c\rho_a d_a^2}\left[\frac{m_a R_a T}{2\pi} \times \frac{m_a + m_{HNO3}}{m_{HNO3}}\right]^{\frac{1}{2}} \quad [S35]$$

$$\lambda = \frac{3D_g}{\upsilon} = \frac{3D_g}{\sqrt{\frac{8R_a T}{\pi m_{HNO3}}}} \quad [S36]$$

$$K_n = \frac{2\lambda}{D} \quad [S37]$$

$$k_{HNO3} = \frac{2\pi D D_g}{1 + \frac{4K_n}{3\gamma} \times \left(1 - \frac{0.47\gamma}{1 + K_n}\right)} \quad [S38]$$

For sea-salt, the diameter (D) in Eqs S37 and S38 refers to the dry modal-mean diameter $D_{SS,r}e^{0.5\ln^2\sigma_r}$ multiplied by a relative-humidity dependent growth factor which ranges from 1.442 at RH=40% to 2.876 at RH=95%. For dust, the diameter (D) in Eqs S37 and S38 refers to the geometric mean diameter for each bin ($D_{du,b}$= 0.28, 0.88, 2.8, 8.8, 28 μm for bins $b = 2, \ldots, 6$ respectively). For sea-salt, $\gamma = \gamma_{SS}$ in Eq. S38, while for dust $\gamma = \gamma_{du}$.

The above algorithm delivers condensation rates for sea-salt ($k_{SS,r}$ for $r = 2,3$) and dust ($k_{du,b}$ for $b = 2, \ldots, 6$). A Ca^{2+} limitation is now applied as in Hauglustaine *et al.* (2014), where the assumption is made that the Ca^{2+} content of dust is invariant at 5%.

S2.5 Map NO_3 uptake to accumulation and coarse soluble modes

The existing UKCA dust scheme utilises the CLASSIC dust emissions scheme and the mapping between the 6 CLASSIC bins and 2 UKCA modes is such that mass from bin 2 and half of bin 3 is mapped to the accumulation mode, while half of bin 3 and bins 4 and 5 are mapped to the coarse mode. The same mapping ratios are utilised here, with the exception that NO_3 uptake on bin 6 (super coarse dust sizes) is also mapped to the coarse soluble mode. The *Nk* rates (s^{-1}) defined in Section S1.2 (Eqs S13-S14) are determined for dust, sea-salt and then a composite.

$$Nk_{du,ACC} = N_{du,2}k_{du,2} + 0.5 \times N_{du,3}k_{du,3} \quad [S39]$$

$$Nk_{du,COA} = 0.5 \times N_{du,3}k_{du,3} + N_{du,4}k_{du,4} + N_{du,5}k_{du,5} + N_{du,6}k_{du,6} \quad [S40]$$

$$Nk_{SS,ACC} = N_{SS,1}k_{SS,1} \quad [S41]$$

$$Nk_{SS,COA} = N_{SS,2}k_{SS,2} \quad [S42]$$

$$Nk_{ACC} = Nk_{du,ACC} \times \frac{m_{Ca(NO3)2}}{m_{HNO3}} + Nk_{SS,ACC} \times \frac{m_{NaNO3}}{m_{HNO3}} \quad [S43]$$

$$Nk_{COA} = Nk_{du,COA} \times \frac{m_{Ca(NO3)2}}{m_{HNO3}} + Nk_{SS,COA} \times \frac{m_{NaNO3}}{m_{HNO3}} \quad [S44]$$

The molar masses in Eqs S43-S44 are $m_{HNO3} = 0.063$ kg mol^{-1}, $m_{NaNO3} = 0.084$ kg mol^{-1} and $m_{Ca(NO3)2} = 0.164$ kg mol^{-1}.

The total coarse mode nitrate mass tendency (using the notation of [*X*] to represent mass concentration of substance *X*) is thus defined as:

$$\frac{\Delta[\mathrm{hetNO_3}]}{\Delta t} = (Nk_{ACC} + Nk_{COA}) \times [\mathrm{HNO_3}] \quad [S45]$$

The nitric acid tendency is now defined as:

$$\frac{\Delta[\mathrm{HNO_3}]}{\Delta t} = -\left(2 \times \left(Nk_{du,ACC} + Nk_{du,COA}\right) + \left(Nk_{SS,ACC} + Nk_{SS,COA}\right)\right) \times [\mathrm{HNO_3}] \quad [S46]$$

Note that the dust rates are doubled in Eq. S46 to account for the 2 moles of HNO_3 required to produce one mole of $Ca(NO_3)_2$.

At this point in the algorithm $\frac{\Delta[\mathrm{hetNO_3}]}{\Delta t}$ is adjusted (if necessary) to ensure that HNO_3 concentrations after the timestep remain above or equal to zero. The modal nitrate mass tendency is then determined:

$$\frac{\Delta[\mathrm{hetNO_3}]_{ACC}}{\Delta t} = \frac{\Delta[\mathrm{hetNO_3}]}{\Delta t} \times \frac{Nk_{ACC}}{Nk_{ACC} + Nk_{COA}} \quad [S48]$$

$$\frac{\Delta[\mathrm{hetNO_3}]_{COA}}{\Delta t} = \frac{\Delta[\mathrm{hetNO_3}]}{\Delta t} \times \frac{Nk_{COA}}{Nk_{ACC} + Nk_{COA}} \quad [S49]$$

S2.6 Determine sea-salt mass tendency and tidy up

The modal sea-salt mass tendency (for modes $r = 2,3$ or the accumulation and coarse soluble modes) is now calculated. Currently, the chlorine ion (Cl^-) associated with Na^+ is simply removed from the aerosol and replaced with NO_3.

$$\frac{\Delta[\mathrm{SS}]_r}{\Delta t} = -N_{SS,r} k_{SS,r} \times \frac{m_{NaCl}}{m_{HNO3}} \times [\mathrm{HNO_3}] \quad [S50]$$

At present, UKCA does not allow 2-way feedback with non-UKCA UM fields, thus the CLASSIC dust concentrations cannot be altered in a similar manner to sea-salt (Eq. S50). However, the UKCA-mode dust scheme will eventually supersede CLASSIC dust and will readily allow for such feedback.

As with the ammonium nitrate production scheme, NH_3 and HNO_3 mass concentrations are updated at the end of the module.

S3 UKCA-mode emissions inventory

This section provides further detail on UKCA-mode gas and aerosol emissions used in the MetUM integrations performed for this study. All emissions are based on constant year 2000 conditions. Global totals are provided in Table S2 for each species emitted via ancillary files.

Oceanic DMS emissions utilise the monthly sea-water concentration climatology of Kettle *et al*. (1999) coupled to the sea-air exchange scheme of Liss and Merlivat (1986), while land DMS emissions follow Spiro *et al*. (1992). On an annual mean basis, total DMS emissions amount to 29 Tg[S] yr^{-1}. Anthropogenic SO_2 emissions from the CEDS inventory are divided into 'chimney-top' high-level emissions at 0.5 km altitude and surface-level emissions [Sellar *et al*., 2020]. A fixed fraction of SO_2 emissions (2.5%) are emitted as primary SO_4 aerosol following AeroCom recommendations (Dentener *et al*., 2006). Natural SO_2 emissions from passive volcanic eruptions also follow Dentener *et al*. (2006). In total, global SO_2 emissions amount to 140 Tg yr^{-1}, of which 74% is anthropogenic.

Primary sea-salt emissions are driven by the simulated surface-wind speed at each time-step using the Gong-Monahan sea-spray source function (Gong, 2003). On an annual mean basis, total sea-salt emissions amount to ~4040 Tg yr^{-1} (of which 4016 Tg yr^{-1} is in the coarse mode), while primary SO_4 aerosol emissions amount to 1.6 Tg[S] yr^{-1}. Primary marine OM emissions follow the parameterisation of Gantt *et al.* (2011) based on surface-wind speed and chlorophyll, while secondary OM is produced from the atmospheric oxidation of monoterpenes from land-sources (Mulcahy *et al.*, 2020). In total, global BC emissions amount to 9.8 Tg[C] yr^{-1} while OM production amounts to 54 Tg[C] yr^{-1}. Secondary SO_4 aerosol is produced in the atmosphere via condensational uptake of H_2SO_4 aerosol on pre-existing aerosol (25 Tg[S] yr^{-1} on a global basis from these simulations), aqueous phase SO_2 oxidation by H_2O_2 and O_3 in cloud droplets (23.7 Tg[S] yr^{-1}), and by binary homogeneous nucleation (0.4 Tg[S] yr^{-1}).

References

Ackermann, I. J., Hass, H., Memmesheimer, M., Ziegenbein, C., and Ebel, A.: The parameterization of the sulfate-nitrate ammonia aerosol system in the long-range transport model EURAD, Meteorol. Atmos. Phys., 57, 101–114, 1995.

Archibald, A. T., O'Connor, F. M., Abraham, N. L., Archer-Nicholls, S., Chipperfield, M. P., Dalvi, M., Folberth, G. A., Dennison, F., Dhomse, S. S., Griffiths, P. T., Hardacre, C., Hewitt, A. J., Hill, R. S., Johnson, C. E., Keeble, J., Köhler, M. O., Morgenstern, O., Mulcahy, J. P., Ordóñez, C., Pope, R. J., Rumbold, S. T., Russo, M. R., Savage, N. H., Sellar, A., Stringer, M., Turnock, S. T., Wild, O., and Zeng, G.: Description and evaluation of the UKCA stratosphere–troposphere chemistry scheme (StratTrop vn 1.0) implemented in UKESM1, Geosci. Model Dev., 13, 1223–1266, https://doi.org/10.5194/gmd-13-1223-2020, 2020.

Dentener, F., Kinne, S., Bond, T., Boucher, O., Cofala, J., Generoso, S., Ginoux, P., Gong, S., Hoelzemann, J. J., Ito, A., Marelli, L., Penner, J. E., Putaud, J. P., Textor, C., Schulz, M., van der Werf, G. R., and Wilson, J.: Emissions of primary aerosol and precursor gases in the years 2000 and 1750, prescribed data-sets for AeroCom., Atmos. Chem. Phys., 6, 4321–4344, 2006.

Fairlie, T. D., Jacob, D. J., Dibb, J. E., Alexander, B., Avery, M. A., van Donkelaar, A., and Zhang, L.: Impact of mineral dust on nitrate, sulfate, and ozone in transpacific Asian pollution plumes, Atmos. Chem. Phys., 10, 3999–4012, doi:10.5194/acp-10-3999-2010, 2010.

Feng, Y., and J. E. Penner (2007), Global modeling of nitrate and ammonium: Interaction of aerosols and tropospheric chemistry, J. Geophys. Res., 112, D01304, doi:10.1029/2005JD006404.

Fuchs, N. A. and Sutugin, A. G.: Highly Dispersed Aerosols, Butterworth-Heinemann, Newton, Mass., USA, 105, 1970.

Gantt, B., Meskhidze, N., Facchini, M. C., Rinaldi, M., Ceburnis, D., and O'Dowd, C. D.: Wind speed dependent size-resolved parameterization for the organic mass fraction of sea spray aerosol, Atmospheric Chemistry and Physics, 11, 8777–8790, https://doi.org/10.5194/acp-11-8777-2011, https://www.atmos-chem-phys.net/11/8777/2011/, 2011.

Gerber, H. E.: Relative-humidity parameterization of the Navy Aerosol Model (NAM), NRL Report 8956, Naval Research Laboratory, Washington, DC, 1985.

Giorgi, F.: Climate change hot-spots, Geophys. Res. Lett., 33, L08707, https://doi.org/10.1029/2006GL025734, 2006.

Gong, S. L.: A parameterization of sea-salt aerosol source function for sub- and super- micron particles, Global Biogeochem. Cycles, 17(4), 1097, doi:1029/2003GB002079, 2003.

Hauglustaine, D. A., Y. Balkanski, and M. Schulz (2014), A global model simulation of present and future nitrate aerosols and their direct radiative forcing of climate, Atmos. Chem. Phys., 14, 11,031–11,063.

Kettle, A., Andreae, M. O., Amouroux, D., Andreae, T. W., Bates, T. S., Berresheim, H., Bingemer, H., Boniforti, R., Curran, M. A. J., DiTullio, G. R., Helas, G., Jones, G. B., Keller, M. D., Kiene, R. P., Leck, C., Levasseur, M., Malin, G., Maspero, M., Matrai, P., McTaggart, A. R., Mihalopoulos, N., Nguyen, B. C., Novo, A., Putaud, J. P., Rapsomanikis, S., Roberts, G., Schebeske, G., Sharma, S., Simo, R., Staubes, R., Turner, S., and Uher, G.: A ´ global database of sea surface dimethylsulfide (dms) measurements and a method to predict sea surface dms as a function of latitude, longitude and month, Global Biogeochem. Cycles, 13, 399–444, 1999.

Liss, P. S. and Merlivat, L.: Air-sea gas exchange rates: introduction and synthesis, in: The role of air-sea exchange in geochemical cycling, edited by: Buat-Menard, P., D. Reidel Publishing Company, 113–127, 1986

Makar, P. A., H. A. Wiebe, R. M. Staebler, S. M. Li, and K. Anlauf (1998), Measurement and modeling of particle nitrate formation, J. Geophys. Res., 103, 13,095–13,110.

Metzger, S., Dentener, F., Pandis, S., and Lelieveld, J.: Gas/aerosol partitioning: 1. A computationally efficient model, J. Geophys. Res., 107, 4312, doi:10.1029/2001JD001102, 2002

Mozurkewich, M.: The dissociation constant of ammonium nitrate and its dependence on temperature, relative humidity and particle size, Atmos. Environ. A-Gen., 27, 261–270, 1993

Mulcahy, J. P., Johnson, C., Jones, C. G., Povey, A. C., Scott, C. E., Sellar, A., Turnock, S. T., Woodhouse, M. T., Abraham, N. L., Andrews, M. B., Bellouin, N., Browse, J., Carslaw, K. S., Dalvi, M., Folberth, G. A., Glover, M., Grosvenor, D. P., Hardacre, C., Hill, R., Johnson, B., Jones, A., Kipling, Z., Mann, G., Mollard, J., O'Connor, F. M., Palmiéri, J., Reddington, C., Rumbold, S. T., Richardson, M., Schutgens, N. A. J., Stier, P., Stringer, M., Tang, Y., Walton, J., Woodward, S., and Yool, A.: Description and evaluation of aerosol in UKESM1 and HadGEM3-GC3.1 CMIP6 historical simulations, Geosci. Model Dev., 13, 6383–6423, https://doi.org/10.5194/gmd-13-6383-2020, 2020.

Schwartz, S. E.: Mass transport considerations pertinent to aqueous phase reactions of gases in liquid-water clouds, in: Chemistry of Multiphase Atmospheric Systems, edited by: Jaeschke, W., 415–471, Springer, New York, 1986.

Seinfeld, J. H., and Pandis, S. N.: Atmospheric chemistry and Physics, John Wiley and Sons, New York, 1998

Sellar, A., Walton, J., Jones, C. G., Wood, R., Abraham, N. L., Andrejczuk, M., Andrews, M. B., Andrews, T., Archibald, A. T., Dyson, H., Elkington, M., Ellis, R., Florek, P., Good, P., Gohar, L.,

Haddad, S., Hardiman, S. C., Hogan, E., Iwi, A., Jones, C. D., Johnson, B., Kelley, D. I., Kettleborough, J., Knight, J. R., Köhler, M. 5 O., Kuhlbrodt, T., Liddicoat, S., Linova-Pavlova, I., Mizielinski, M. S., Morgenstern, O., Mulcahy, J., Neininger, E., O'Connor, F. M., Petrie, R., Ridley, J., Rioual, J.-C., Roberts, M., Robertson, E., Rumbold, S., Seddon, J., Shepherd, H., Shim, S., Stephens, A., Teixeira, J. C., Tang, Y., Williams, J., and Wiltshire, A.: Implementation of UK Earth system models for CMIP6, J. Adv. Model. Earth Syst., 12, e2019MS001946. https://doi.org/10.1029/2019MS001946, 2020.

Spiro, P. A., Jacob, D. J., and Logan, J. A.: Global inventory of sulfur emissions with 1◦×1 ◦ resolution, J. Geophys. Res., 97, 6023–6036, 1992.

Wang, B., and A. Laskin (2014), Reactions between water-soluble organic acids and nitrates in atmospheric aerosols: Recycling of nitric acid and formation of organic salts, J. Geophys. Res. Atmos., 119, 3335–3351, doi:10.1002/2013JD021169

Woodward, S.: Modelling the atmospheric life cycle and radiative impact of mineral dust in the Hadley Centre climate model, J. Geophys. Res., 106, D16, 18155–18166, 2001.

Reaction type	Reaction	Net global tropospheric HNO_3 production (Tg[N] yr^{-1})	
		FAST	SLOW
Bimolecular	$N_2O_5 + H_2O \rightarrow 2HNO_3$	0.78	0.84
Bimolecular	$NO_3 + EtCHO \rightarrow HNO_3 + EtCO_3$	0.007	0.007
Bimolecular	$NO_3 + HCHO \rightarrow HNO_3 + HO_2 + CO$	0.13	0.13
Bimolecular	$NO_3 + MGLY \rightarrow HNO_3 + MeCO_3 + CO$	0.029	0.031
Bimolecular	$NO_3 + Me_2CO \rightarrow HNO_3 + MeCOCH_2OO$	0.017	0.018
Bimolecular	$NO_3 + MeCHO \rightarrow HNO_3 + MeCO_3$	0.061	0.064
Bimolecular	$HNO_3 + OH \rightarrow NO_3 + H_2O$	-6.2	-6.3
Bimolecular	$DMS + NO_3 \rightarrow SO_2 + HNO_3 + MeOO$	2.3	2.3
Termolecular	$OH + NO_2 \rightarrow HNO_3 + m$	31.9	32.3
Photolysis	$HNO_3 + h\nu \rightarrow NO_2 + OH$	-3.4	-3.4
Het. PSC/NAT	$ClONO_2 + H_2O \rightarrow HNO_3 + HCl$	0.86	0.84
Het. PSC/NAT	$ClONO_2 + HCl \rightarrow HNO_3 + 2Cl$	0.11	0.11
Het. PSC/NAT	$N_2O_5 + HCl \rightarrow HNO_3 + NO_2 + Cl$	0.001	0.001
Het. PSC/NAT/Aero	$N_2O_5 + H_2O \rightarrow 2HNO_3$	17.6	17.3
	Total	44.15	44.18

Table S1: Chemical reactions in UKCA StratTrop1.0 that involve nitric acid (HNO_3), and net annual and global tropospheric HNO_3 production (Tg[N] yr^{-1}) in the FAST and SLOW simulations. See Archibald *et al.* (2020) for details of the chemical species

Species	Source	Time	Domain	Units	Emissions
BC	Biofuel	Monthly	Surface	Tg[C] yr^{-1}	3.1
BC	Fossil fuel	Monthly	Surface	Tg[C] yr^{-1}	2.9
BC	Biomass high level	Monthly	Surface	Tg[C] yr^{-1}	1.2
BC	Biomass surface	Monthly	Surface	Tg[C] yr^{-1}	2.6
C_2H_6	Biogenic	Monthly	Surface	Tg yr^{-1}	31.1
C_2H_6	Oceanic	Monthly	Surface	Tg yr^{-1}	2.4
C_2H_6	Anthropogenic	Monthly	Surface	Tg yr^{-1}	13.8
C_2H_6	Biomass	Monthly	Surface	Tg yr^{-1}	10.7
C_3H_8	Biogenic	Monthly	Surface	Tg yr^{-1}	15.6
C_3H_8	Oceanic	Monthly	Surface	Tg yr^{-1}	2.8
C_3H_8	Anthropogenic	Monthly	Surface	Tg yr^{-1}	9.2
C_3H_8	Biomass	Monthly	Surface	Tg yr^{-1}	5.2
C_5H_8	Biogenic	Monthly	Surface	Tg yr^{-1}	568
CH_4	Biomass	Monthly	Surface	Tg yr^{-1}	18.8
CO	Biogenic	Monthly	Surface	Tg yr^{-1}	88.6
CO	Oceanic	Monthly	Surface	Tg yr^{-1}	19.6
CO	Anthropogenic	Monthly	Surface	Tg yr^{-1}	594
CO	Biomass	Monthly	Surface	Tg yr^{-1}	401
DMS	Land	Monthly	Surface	Tg[S] yr^{-1}	0.9
DMS	Biomass	Monthly	Surface	Tg[S] yr^{-1}	0.01
HCHO	Biogenic	Monthly	Surface	Tg yr^{-1}	4.6
HCHO	Anthropogenic	Monthly	Surface	Tg yr^{-1}	2.3
HCHO	Biomass	Monthly	Surface	Tg yr^{-1}	5.5
Me_2CO	Biogenic	Monthly	Surface	Tg yr^{-1}	37.4
Me_2CO	Anthropogenic	Monthly	Surface	Tg yr^{-1}	2.6
Me_2CO	Biomass	Monthly	Surface	Tg yr^{-1}	3.5
MeCHO	Biogenic	Monthly	Surface	Tg yr^{-1}	21.5
MeCHO	Anthropogenic	Monthly	Surface	Tg yr^{-1}	1.7
MeCHO	Biomass	Monthly	Surface	Tg yr^{-1}	8.2
Monoterpene	Biogenic	Monthly	Surface	Tg yr^{-1}	94.7
NH_3	Oceanic	Single time	Surface	Tg yr^{-1}	9.8
NH_3	Anthropogenic	Monthly	Surface	Tg yr^{-1}	50.5

NH_3	Biomass	Monthly	Surface	Tg yr^{-1}	4.7
NO_X	Soil	Monthly	Surface	Tg[NO] yr^{-1}	11.8
NO_X	Anthropogenic	Monthly	Surface	Tg[NO] yr^{-1}	76.8
NO_X	Biomass	Monthly	Surface	Tg[NO] yr^{-1}	16.1
NO_X	Aircraft	Monthly	Levels	Tg[NO] yr^{-1}	1.6
NVOC	Biogenic	Monthly	Surface	Tg[C] yr^{-1}	225
NVOC	Anthropogenic	Monthly	Surface	Tg[C] yr^{-1}	6
NVOC	Biomass	Monthly	Surface	Tg[C] yr^{-1}	16.6
OC	Biofuel	Monthly	Surface	Tg[C] yr^{-1}	9.3
OC	Fossil fuel	Monthly	Surface	Tg[C] yr^{-1}	5.3
OC	Biomass high level	Monthly	Surface	Tg[C] yr^{-1}	15.2
OC	Biomass surface	Monthly	Surface	Tg[C] yr^{-1}	18.8
SO_2	Natural	Single time	Levels	Tg yr^{-1}	28.8
SO_2	Anthropogenic high level	Monthly	Surface	Tg yr^{-1}	75
SO_2	Anthropogenic surface	Monthly	Surface	Tg yr^{-1}	36.6

Table S2: Prescribed UKCA aerosol and gas emissions for the MetUM simulations with temporal and domain specifications and global and annual total emissions in given units

Wavelength λ (μm)	n(λ)	k(λ)
0.1051	1.427	0.3985
0.106	1.439	0.3975
0.1069	1.4535	0.3935
0.1078	1.4635	0.3875
0.1088	1.4715	0.376
0.1097	1.4775	0.363
0.1107	1.4825	0.347
0.1117	1.483	0.3345
0.1127	1.4795	0.3305
0.1137	1.4795	0.3395
0.1148	1.4765	0.355
0.1159	1.484	0.346
0.117	1.5175	0.3495
0.1181	1.5565	0.3565
0.1192	1.602	0.345
0.1204	1.6295	0.30255
0.1216	1.642	0.2332
0.1228	1.6405	0.1898
0.124	1.6165	0.16375
0.1252	1.5955	0.154276
0.1265	1.577	0.144013
0.1278	1.5685	0.13375
0.1292	1.5585	0.1271
0.1305	1.5545	0.11375
0.1319	1.5495	0.1036
0.1333	1.54	0.0901
0.1348	1.5295	0.0714
0.1362	1.513	0.058895
0.1378	1.492	0.045915
0.1393	1.472	0.040195
0.1409	1.46	0.0458
0.1425	1.4515	0.04975
0.1442	1.4495	0.0464
0.1459	1.446	0.03965
0.1476	1.4405	0.033905
0.1494	1.4265	0.02473
0.1512	1.412	0.02157
0.1531	1.3955	0.018235
0.155	1.379	0.0149
0.1569	1.3545	0.015265
0.159	1.33	0.01768
0.161	1.2995	0.02548
0.1631	1.2735	0.03367
0.1653	1.2465	0.04965
0.1675	1.218	0.07143
0.1698	1.19	0.09385
0.1722	1.156	0.13415
0.1746	1.1455	0.17445
0.1771	1.137	0.2282
0.1797	1.144	0.299
0.1823	1.167	0.3565
0.1851	1.199	0.4045
0.1879	1.239	0.4375
0.1907	1.3015	0.46385
0.1937	1.362	0.471
0.1968	1.425	0.4946
0.2	1.4575	0.46865
0.2033	1.5055	0.466
0.2066	1.549	0.4565
0.2101	1.5985	0.4487
0.2138	1.6685	0.4281
0.2175	1.7375	0.3837
0.2214	1.787	0.29235
0.2254	1.804	0.170785
0.2296	1.766	0.174
0.2339	1.712	0.0806
0.2384	1.6615	0.0358
0.2431	1.624	0.0212

0.248	1.5925	0.0109
0.253	1.572	0.0028
0.2583	1.55	0.007121
0.2638	1.5365	0.003526
0.2695	1.52	0.00239
0.2755	1.5095	0.001996
0.2818	1.502	0.001926
0.2883	1.498	0.001941
0.2952	1.492	0.002063
0.3024	1.489	0.00237
0.31	1.4875	0.002933
0.32	1.488986	0.004039
0.33	1.490471	0.005925
0.34	1.491957	0.00797
0.35	1.493442	0.009556
0.36	1.494928	0.010146
0.37	1.496413	0.008971
0.38	1.497899	0.005179
0.39	1.499384	0.002114
0.4	1.50087	0.000979
0.405	1.49953	0.00069
0.41	1.49826	0.000466
0.415	1.49702	0.000266
0.42	1.49583	9.22E-05
0.44	1.49148	1.00E-08
0.46	1.48766	1.00E-08
0.48	1.48432	1.00E-08
0.5	1.48139	1.00E-08
0.52	1.47876	1.00E-08
0.535	1.47699	1.00E-08
0.5876	1.465193	1.00E-08
0.656	1.45655	1.00E-08
0.706	1.456074	1.48E-08
0.8	1.457231	1.06E-07
1	1.459694	3.15E-06

1.07	1.459327	1.57E-06
1.15	1.458942	8.06E-06
1.2	1.458725	1.08E-05
1.3	1.458331	1.34E-05
1.4	1.457978	0.000151
1.5	1.457524	0.000199
1.58	1.457128	0.00011
1.6	1.45703	0.000958
1.7	1.456525	6.82E-05
1.8	1.456	0.000123
1.9	1.455475	0.00126
2	1.45495	0.00108
2.17	1.453634	0.00275
2.22	1.453247	0.00567
2.27	1.45286	0.00191
2.3	1.452627	0.00588
2.33	1.452395	0.00196
2.38	1.452008	0.001
2.44	1.451543	0.00309
2.5	1.451079	0.00317
2.56	1.450446	1.00E-08
2.63	1.449707	0.000884
2.7	1.448969	0.00113
2.78	1.448125	0.00951
2.86	1.447279	0.024
2.94	1.446379	0.0553
3.03	1.445367	0.209
3.12	1.444355	0.459
3.2	1.443455	0.507
3.25	1.442893	0.477
3.27	1.442668	0.418
3.32	1.442105	0.425
3.36	1.441485	0.416
3.37	1.44131	0.358
3.39	1.440959	0.311

3.43	1.440257	0.28
3.45	1.439906	0.274
3.47	1.439555	0.239
3.51	1.438853	0.209
3.55	1.438151	0.17
3.57	1.4378	0.15
3.61	1.437115	0.123
3.64	1.436602	0.101
3.7	1.435575	0.0658
3.77	1.434378	0.0516
3.88	1.432311	0.0343
3.97	1.430281	0.0278
3.98	1.430056	0.0279
4.03	1.428928	0.0357
4.07	1.428026	0.0341
4.14	1.426448	0.0566
4.17	1.425757	0.074
4.18	1.425485	0.104
4.2	1.424941	0.0575
4.26	1.423309	0.0298
4.31	1.421949	0.0185
4.39	1.419773	0.0112
4.55	1.415361	0.0108
4.78	1.406344	0.0206
4.85	1.4036	0.0274
4.9	1.40164	0.0211
4.95	1.399679	0.0257
5.11	1.391782	0.0433
5.15	1.389623	0.0437
5.26	1.383685	0.0393
5.46	1.369257	0.0484
5.56	1.361898	0.0613
5.62	1.355779	0.062
5.65	1.35272	0.0773
5.68	1.349661	0.29

5.73	1.344563	0.108
5.8	1.337425	0.141
5.882	1.329063	0.0044
6.061	1.29893	0.0063
6.25	1.258789	0.0098
6.452	1.188639	0.018
6.667	1.048479	0.043
6.711	0.993446	0.058
6.757	0.918412	0.086
6.803	0.808378	0.18
6.812	0.783371	0.24
6.821	0.763365	0.28
6.831	0.748357	0.34
6.84	0.73835	0.4
6.849	0.733344	0.46
6.859	0.728336	0.51
6.868	0.72333	0.56
6.873	0.723326	0.59
6.878	0.723322	0.61
6.882	0.723319	0.64
6.887	0.728315	0.66
6.892	0.733312	0.68
6.897	0.738308	0.71
6.901	0.753305	0.73
6.906	0.768301	0.76
6.911	0.768298	0.78
6.916	0.753294	0.8
6.92	0.738291	0.82
6.925	0.728287	0.84
6.93	0.723283	0.86
6.935	0.72328	0.89
6.944	0.718273	0.93
6.969	0.718254	1.1
6.993	0.718237	1.2
7.018	0.718218	1.3

7.042	0.7232	1.4
7.067	0.728182	1.5
7.092	0.733163	1.7
7.117	0.743144	1.8
7.143	0.753125	2
7.194	0.783087	2.4
7.246	0.853048	3
7.299	1.048009	4.1
7.326	1.332989	5
7.353	2.147969	6.1
7.38	3.762949	4.8
7.407	3.697929	2
7.435	3.212908	0.95
7.463	2.887887	0.56
7.519	2.507845	0.27
7.576	2.297803	0.16
7.634	2.15776	0.11
7.692	2.062717	0.078
7.813	1.932627	0.047
7.937	1.852534	0.031
8.065	1.797439	0.023
8.197	1.752341	0.017
8.333	1.72224	0.013
9.091	1.636676	0.0053
10	1.44	0.0126
11.11	1.4345	0.0142
12.59	1.427	0.0163
14.29	1.416	0.0193
16.67	1.3975	0.0238
20	1.363	0.0315
20.83	1.353	0.0338
21.74	1.341	0.0365
22.73	1.3265	0.0398
23.81	1.3095	0.0437
25	1.288	0.0487

25.64	1.275	0.0518
26.32	1.2605	0.0552
27.03	1.2445	0.0593
27.78	1.226	0.064
28.57	1.2045	0.0697
29.41	1.1795	0.0766
30.3	1.15	0.0852
31.25	1.1145	0.0962
32.26	1.0705	0.111
33.33	1.0165	0.131
34.48	0.947	0.16
35.71	0.8575	0.206
37.04	0.742	0.288
38.46	0.6105	0.456
40	0.521	0.758
41.67	0.522	1.15
43.48	0.654	1.65
44.44	0.8375	1.97
45.45	1.2745	2.35
45.98	1.746	2.56
46.51	2.4935	2.75
47.06	3.1275	2.83
47.62	3.3195	2.68
48.19	3.3275	2.24
48.78	3.218	1.71
50	2.8475	1.01
51.28	2.514	0.763
52.63	2.2655	0.778
54.05	2.1215	0.987
55.56	2.1505	1.25
57.14	2.316	1.21
58.82	2.3805	0.834
60.61	2.3115	0.514
62.5	2.2105	0.333
66.67	2.033	0.179

71.43	1.89	0.126
76.92	1.7575	0.112
80	1.6885	0.115
83.33	1.611	0.127
86.96	1.5205	0.151
90.91	1.4065	0.201
100	1.037	0.625
102.6	0.9375	0.952
105.3	0.8955	1.39
108.1	0.9425	1.9
111.1	1.1535	2.38
114.3	1.61	2.4
117.6	1.9265	1.62
121.2	1.897	0.913
125	1.7875	0.548
133.3	1.6265	0.262
142.9	1.55	0.162
153.8	1.5385	0.118
166.7	1.6295	0.0958
173.9	1.782	0.0888
181.8	2.183	0.0836
190.5	3.437	0.0798
200	4.6385	0.0769
210.5	4.1645	0.0748
222.2	3.733	0.0733
250	3.263	0.0714
285.7	3.0235	0.0704
333.3	2.8815	0.0694
400	2.791	0.0674
500	2.7325	0.0631
578	2.735	0.0162
666.7	2.696	0.0551
751.9	2.715	0.0102
1000	2.6755	0.0418
1075	2.625	0.00618

Table S3: Refractive indices for sodium nitrate ($NaNO_3$). See paper for references.

Wavelength λ (μm)	n(λ)	k(λ)
0.1	1.611	1.00E-08
0.3	1.611	1.00E-08
0.41	1.611	1.00E-08
0.54	1.611	1.00E-08
0.59	1.611	1.00E-08
0.66	1.611	1.00E-08
0.71	1.611	1.48E-08
0.8	1.611	1.06E-07
1	1.611	3.15E-06
1.07	1.611	1.57E-06
1.15	1.611	8.06E-06
1.2	1.611	1.08E-05
1.3	1.611	1.34E-05
1.4	1.611	0.000151
1.5	1.611	0.000199
1.58	1.611	0.00011
1.6	1.611	0.000958
1.7	1.611	6.82E-05
1.8	1.611	0.000123
1.9	1.611	0.00126
2	1.611	0.00108
2.17	1.56	0.00275
2.22	1.55	0.00567
2.27	1.55	0.00191
2.3	1.55	0.00588
2.33	1.55	0.00196
2.38	1.54	0.001
2.44	1.53	0.00309
2.5	1.53	0.00317
2.56	1.51	1.00E-08
2.63	1.5	0.000884
2.7	1.48	0.00113
2.78	1.44	0.00951
2.86	1.4	0.024
2.94	1.31	0.0553
3.03	1.25	0.209
3.12	1.35	0.459
3.2	1.55	0.507
3.25	1.66	0.477
3.27	1.69	0.418
3.32	1.72	0.425
3.36	1.81	0.416
3.37	1.83	0.358
3.39	1.82	0.311
3.43	1.81	0.28
3.45	1.82	0.274
3.47	1.83	0.239
3.51	1.83	0.209
3.55	1.83	0.17
3.57	1.82	0.15
3.61	1.82	0.123
3.64	1.81	0.101
3.7	1.78	0.0658
3.77	1.75	0.0516
3.88	1.71	0.0343
3.97	1.68	0.0278
3.98	1.68	0.0279
4.03	1.67	0.0357
4.07	1.66	0.0341
4.14	1.64	0.0566
4.17	1.64	0.074
4.18	1.64	0.104
4.20	1.7	0.0575
4.26	1.68	0.0298
4.31	1.66	0.0185
4.39	1.65	0.0112
4.55	1.61	0.0108
4.78	1.57	0.0206

4.85	1.57	0.0274
4.9	1.56	0.0211
4.95	1.55	0.0257
5.11	1.53	0.0433
5.15	1.53	0.0437
5.26	1.51	0.0393
5.46	1.46	0.0484
5.56	1.44	0.0613
5.62	1.38	0.062
5.65	1.33	0.0773
5.68	1.35	0.29
5.73	1.49	0.108
5.80	1.45	0.141
5.85	1.43	0.145
5.92	1.44	0.144
6.02	1.42	0.13
6.13	1.39	0.129
6.25	1.33	0.134
6.37	1.27	0.155
6.49	1.17	0.2
6.67	1	0.34
6.76	0.85	0.465
6.85	0.84	0.849
6.99	1.05	1.17
7.04	1.16	1.26
7.14	1.5	1.67
7.17	1.64	1.68
7.19	1.77	1.69
7.34	2.38	1.31
7.46	2.56	0.925
7.69	2.45	0.457
7.81	2.37	0.34
8.20	2.18	0.194
8.47	2.11	0.159
8.62	2.09	0.14

8.93	2.04	0.122
9.1	2.03	0.115
9.35	2.02	0.105
9.45	2.02	0.0749
9.6	2.03	0.0894
9.62	2.02	0.0717
9.80	1.98	0.0642
10	1.95	0.0636
10.2	1.95	0.0649
10.42	1.94	0.0616
10.6	1.94	0.0484
10.66	1.93	0.0459
11.11	1.91	0.038
11.36	1.88	0.027
11.63	1.85	0.0277
11.9	1.62	0.0512
12.05	1.57	0.259
12.16	2.72	0.966
12.2	2.54	0.167
12.24	2.46	0.0313
12.5	1.98	0.00525
13.51	1.89	0.0287
13.74	1.85	0.0351
13.89	1.87	0.0721
13.95	1.88	0.104
14.08	1.94	0.0238
14.29	1.9	0.0181
14.71	1.89	1.00E-08
16.13	1.85	0.0136
17.24	1.84	0.0145
19.23	1.81	0.0244
20	1.82	0.0424
22.2	1.85	0.0136
25	1.85	0.0136
28.6	1.85	0.0136

33.3	1.85	0.0136
40	1.85	0.0136

100000	1	1.00E-08

Table S4: Refractive indices for ammonium nitrate (NH_4NO_3). See paper for references.

				FAST	INSTANT
HNO_3	Source	Gas phase	Tg[N] yr^{-1}	35.2	35.2
		Aerosol phase		18.6	18.6
		Total		53.8	53.7
	Loss	Gas phase	Tg[N] yr^{-1}	9.7	9.6
		Fine nitrate		6.4	6.5
		Coarse nitrate		16.6	16.5
		Dry deposition		6	6
		Wet deposition		14.9	14.7
		Total		53.4	53.3
		Wet fraction	%	71.4	71.2
	Burden		Tg[N]	0.48	0.48
	Lifetime		days	3.2	3.2
NO_3	Source	Fine nitrate	Tg[N] yr^{-1}	6.3	6.5
		Coarse nitrate		16.6	16.5
		Total		22.9	23
	Loss	Dry deposition	Tg[N] yr^{-1}	8.9	8.9
		Wet deposition		14.3	14.4
		Total		21.3	23.2
		Wet fraction	%	61.7	61.9
	Burden	Fine nitrate	Tg[N]	0.11	0.11
		Coarse nitrate		0.09	0.09
		Total		0.2	0.21
	Lifetime	Fine nitrate	days	6.2	6.2
		Coarse nitrate		2	2
		Total		3.2	3.2
NH_3	Source	Emissions	Tg[N] yr^{-1}	53.5	53.5
	Loss	Gas phase	Tg[N] yr^{-1}	-	-
		NH_4 formation		30.4	30.4
		Dry deposition		17.4	17.3
		Wet deposition		5.7	5.6
		Total		53.4	53.4
		Wet fraction	%	24.6	24.5
	Burden		Tg[N]	0.04	0.04
	Lifetime		days	0.28	0.27
NH_4	Source	NH_3 conversion	Tg[N] yr^{-1}	30.4	30.4
	Loss	Dry deposition	Tg[N] yr^{-1}	5.7	5.7
		Wet deposition		24.9	24.9
		Total		30.5	30.6

	Wet fraction	%	81.4	81.4
	Burden	Tg[N]	0.42	0.42
	Lifetime	days	5	5

Table S5: Global and annual-mean metrics for nitric acid (HNO_3), nitrate (NO_3), ammonia (NH_3) and ammonium (NH_4) in the FAST and INSTANT simulations

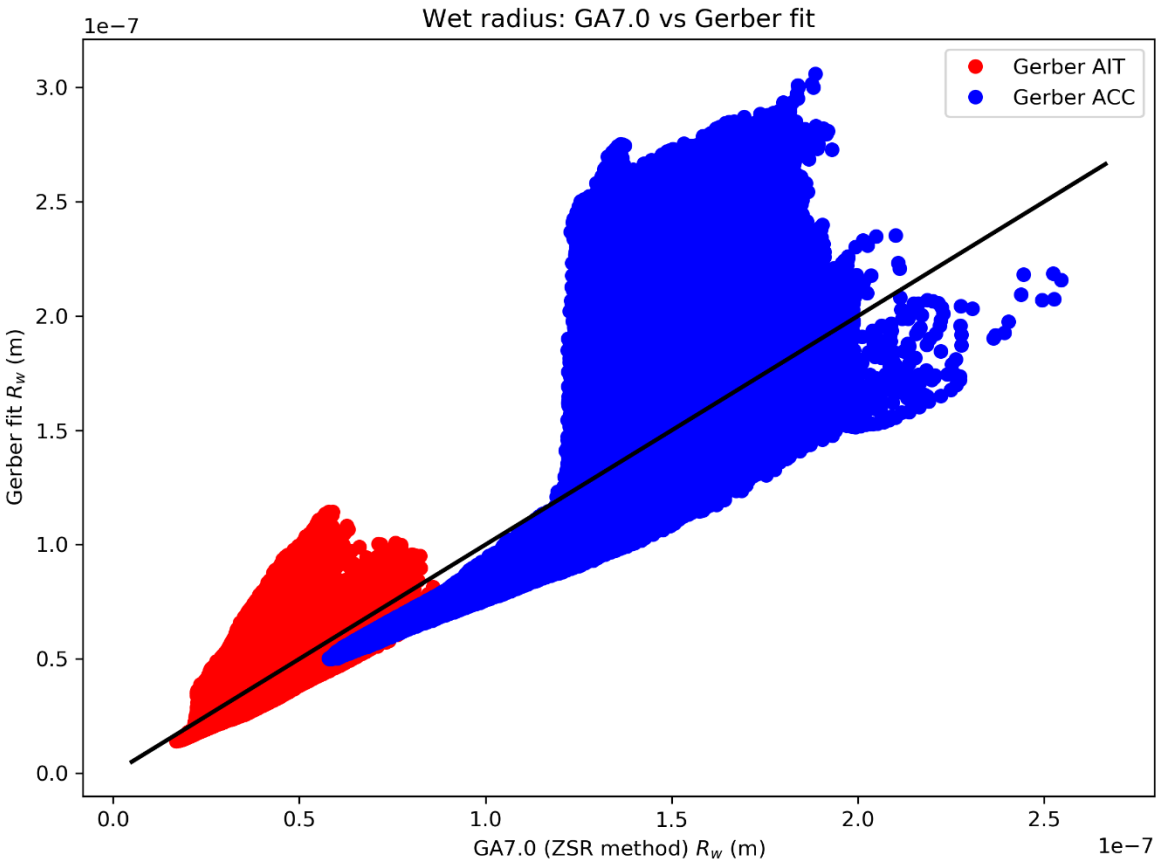

Figure S1: Comparison of wet radii calculated using Gerber's parameterisation applied to annual-mean dry radii, and annual-mean wet diameters using UKCA-mode's ZSR scheme. Results are shown for all grid-cells below the tropopause for a single year of a GA7.0 Met-UM11.5 N96 simulation (year 2000 conditions)

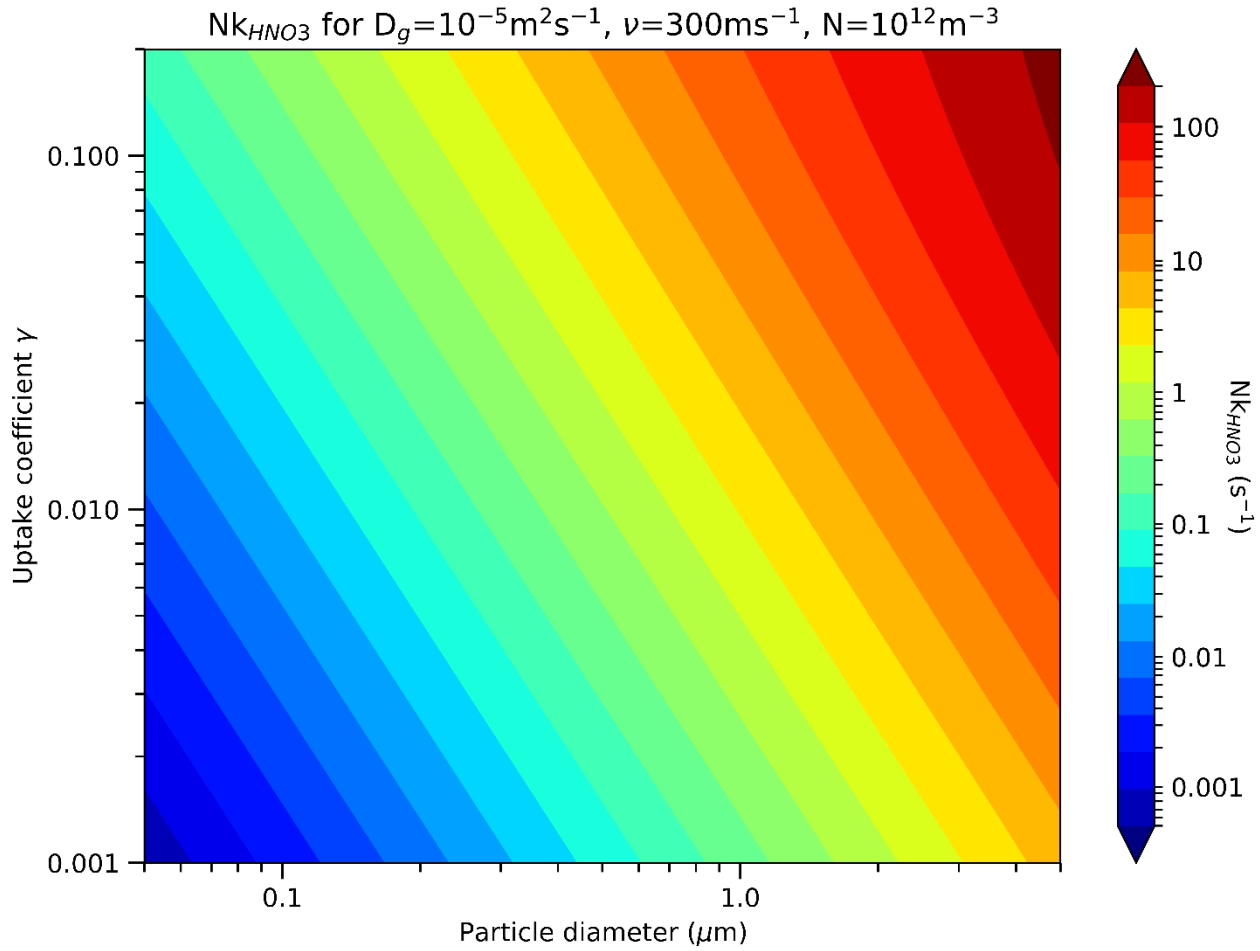

Figure S2: Sensitivity of the uptake rate (k_{HNO3}) in standard atmospheric conditions to the uptake coefficient (γ, ranging from 0.001 to 0.2) and the particle diameter (D, ranging from 0.05 to 0.5 µm), normalised by a particle number concentration of N = 10^{12} m^{-3}. k_{HNO3} is determined using the first order uptake parameterisation (Eqs S9-S12).

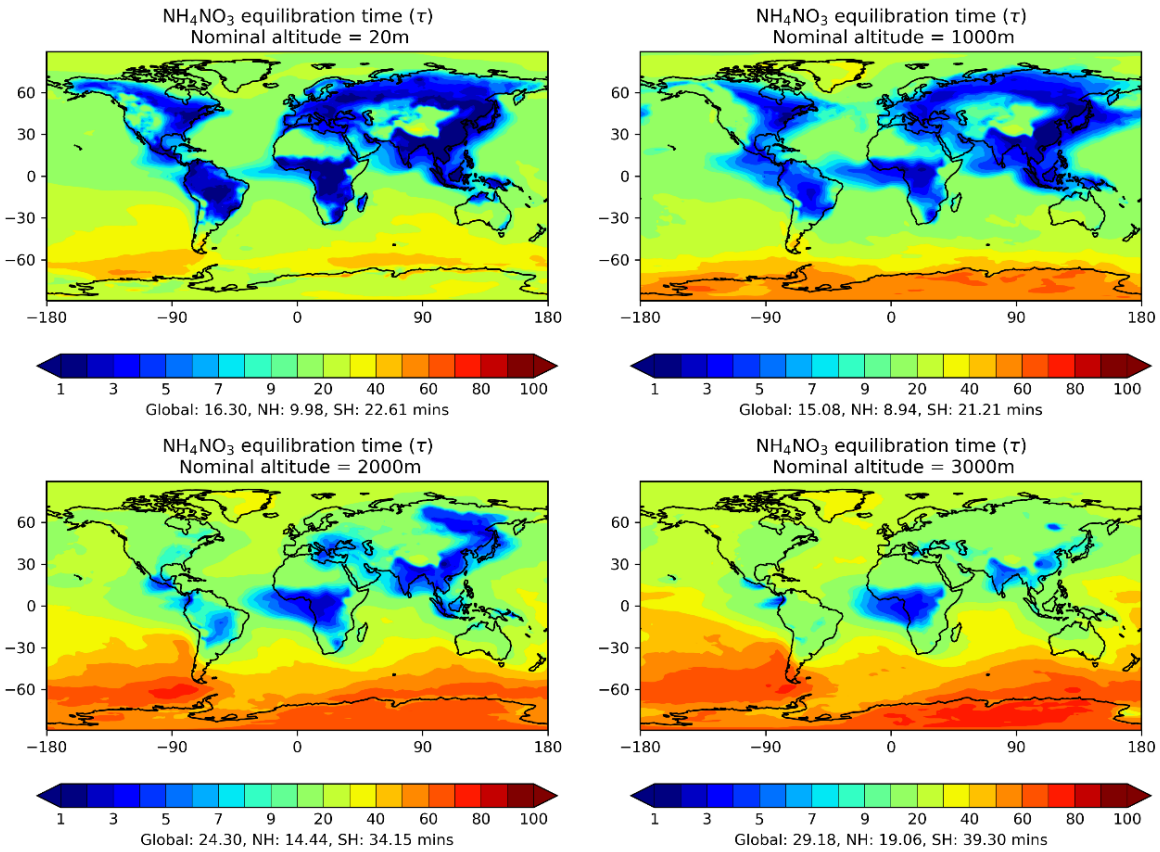

Figure S3: Timescale to reach equilibrium for 4 nominal altitudes determined using output for a single year of a GA7.0 Met-UM11.7 N96 simulation (year 2000 conditions)

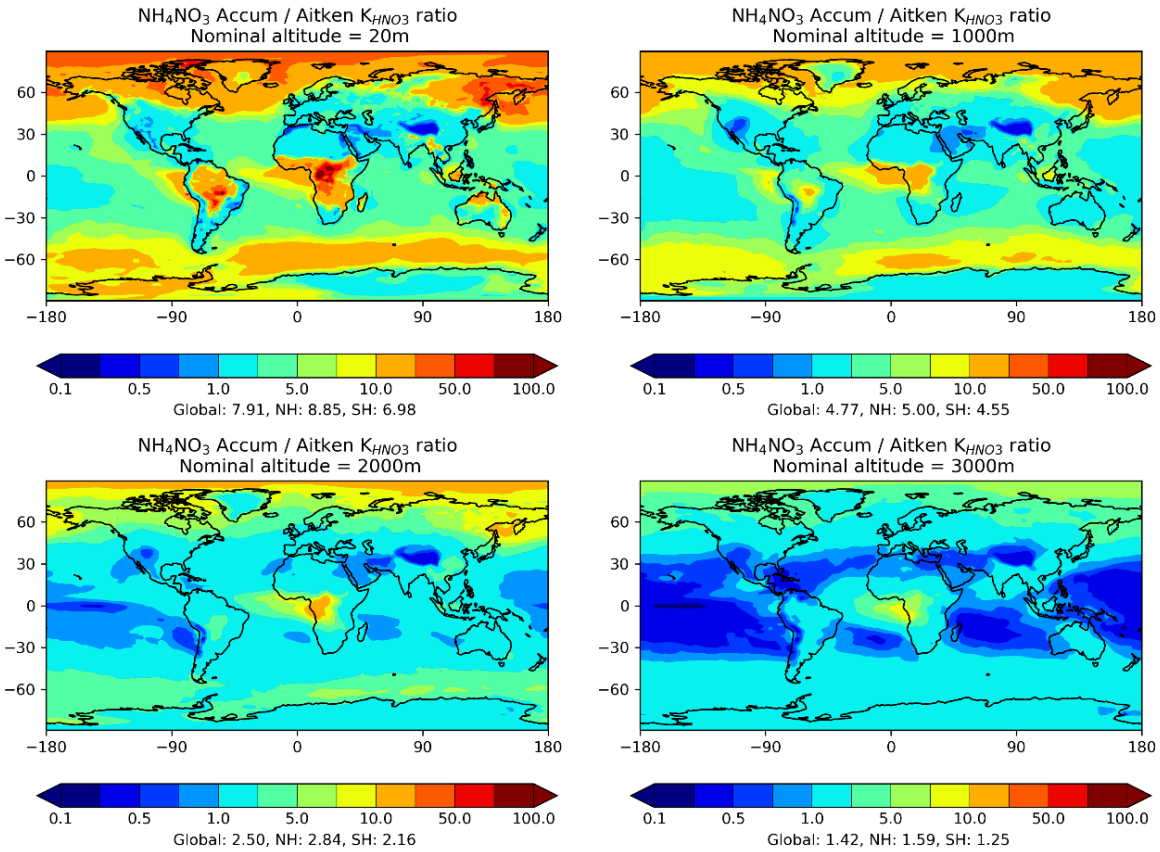

Figure S4: Ratio of Nk_{ACC} to Nk_{AIT} (Eqs S13 and S14) for 4 nominal altitudes determined using output for a single year of a GA7.0 Met-UM11.7 N96 simulation (year 2000 conditions)

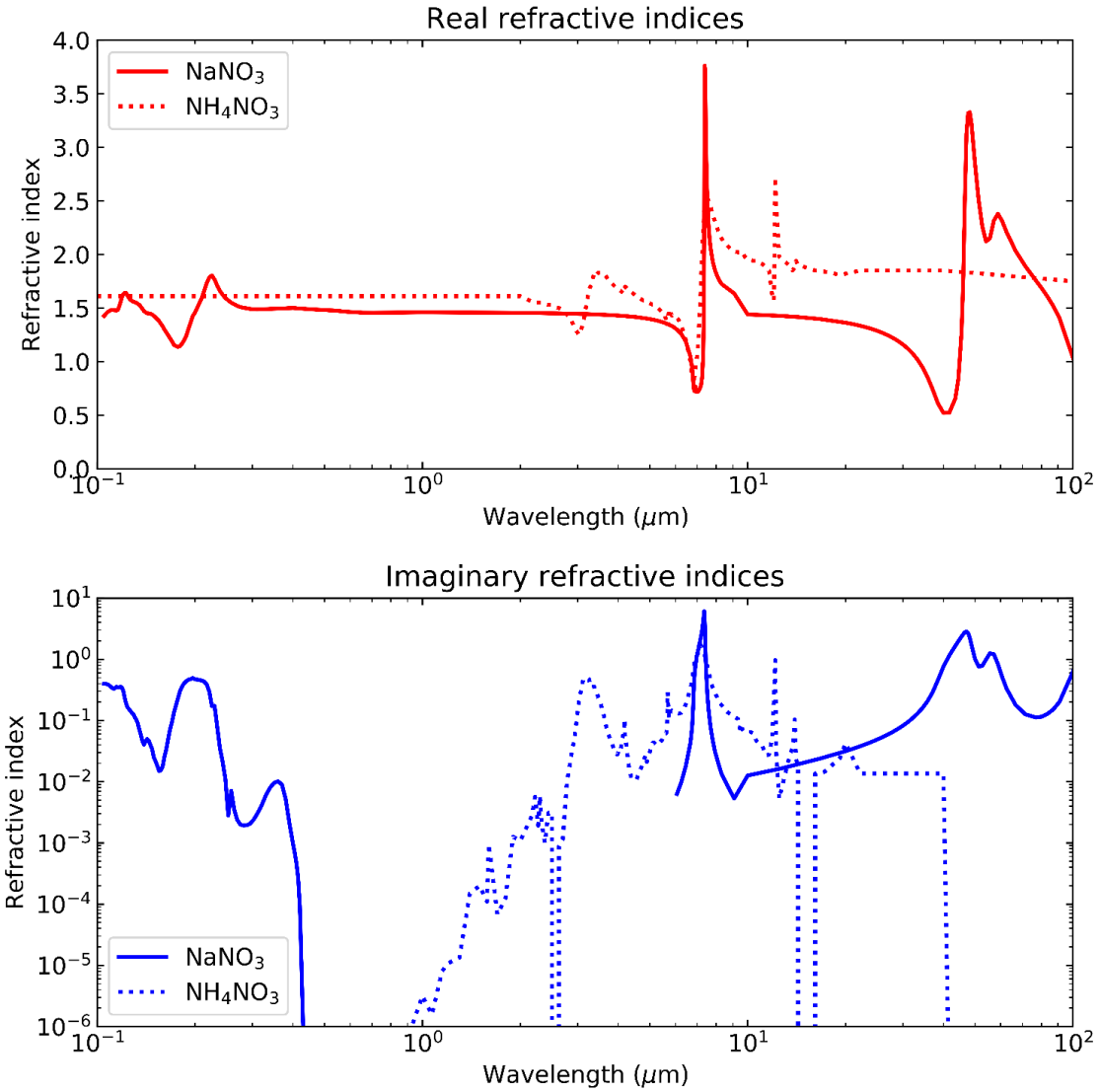

Figure S5: Refractive indices for sodium nitrate ($NaNO_3$) and ammonium nitrate (NH_4NO_3)

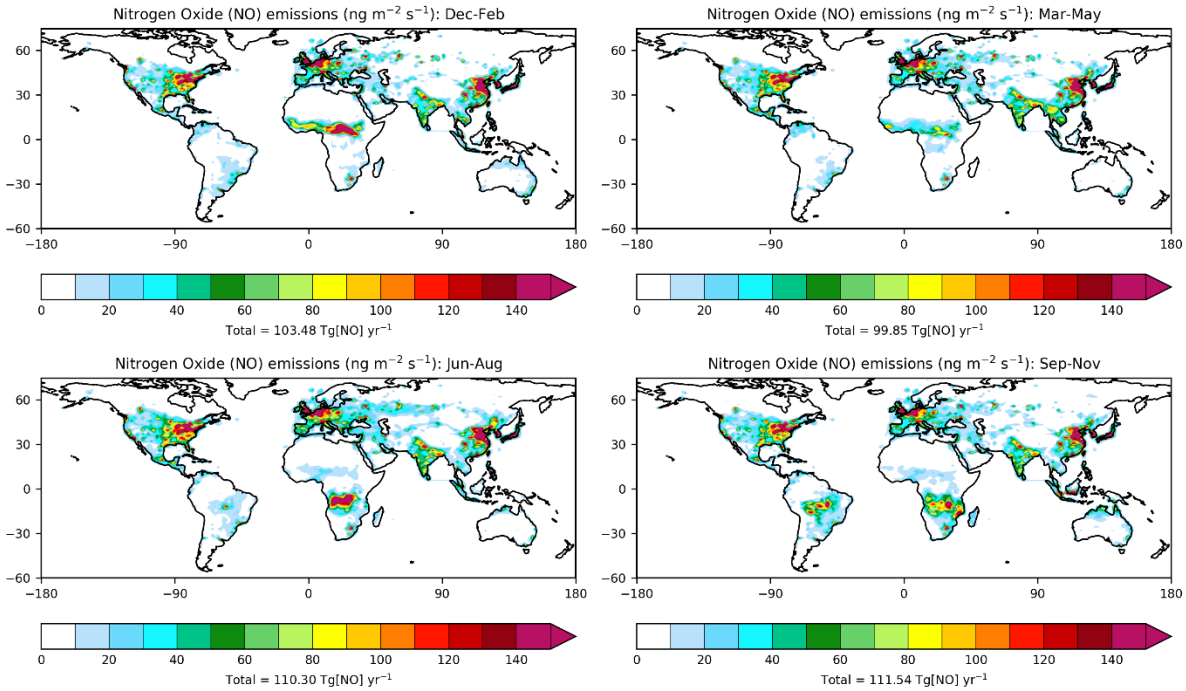

Figure S6a: Seasonal column-integrated nitrogen oxide (NO) emissions in the MetUM simulations

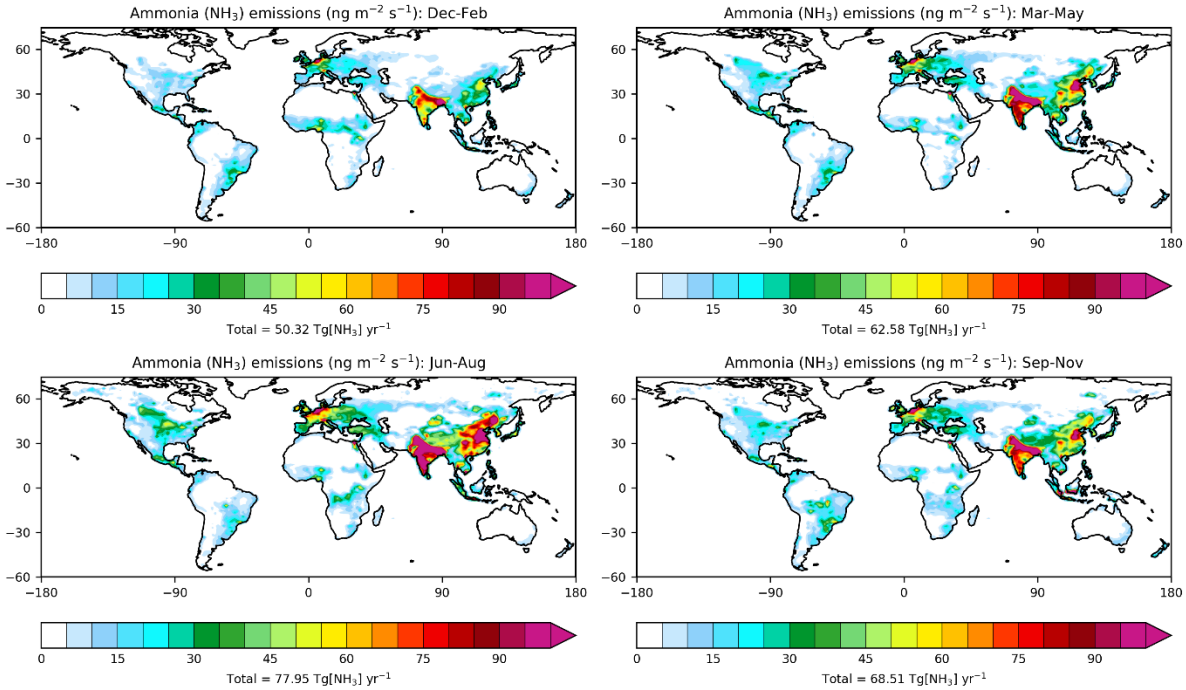

Figure S6b: Seasonal ammonia (NH_3) emissions in the MetUM simulations

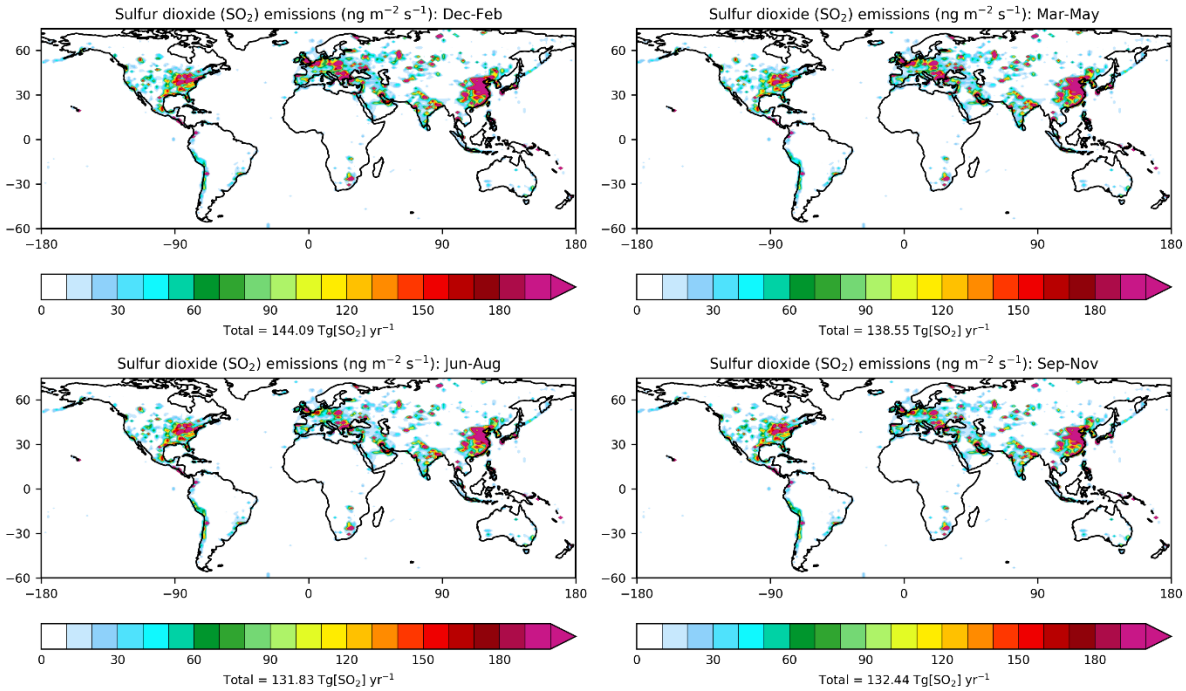

Figure S6c: Seasonal column-integrated sulphur dioxide (SO_2) emissions in the MetUM simulations

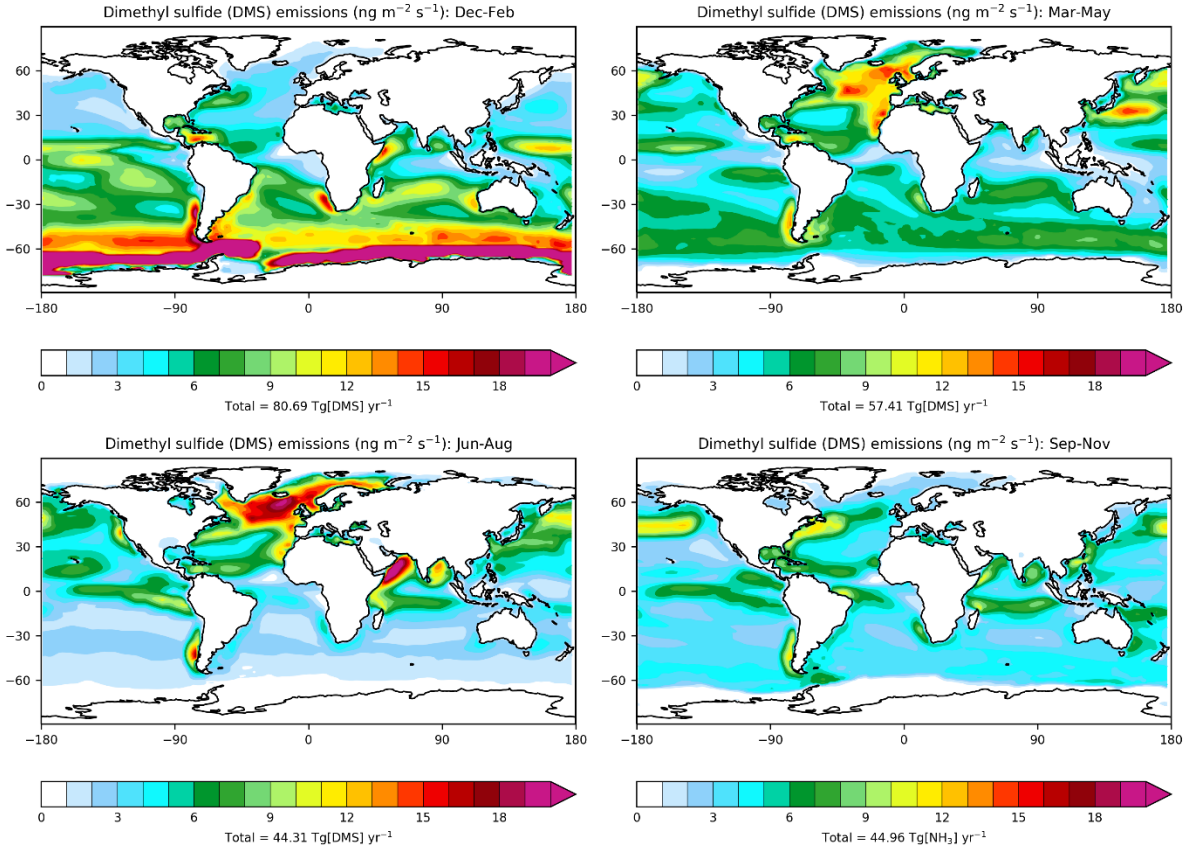

Figure S6d: Seasonal dimethyl sulfide (DMS) emissions in the MetUM simulations

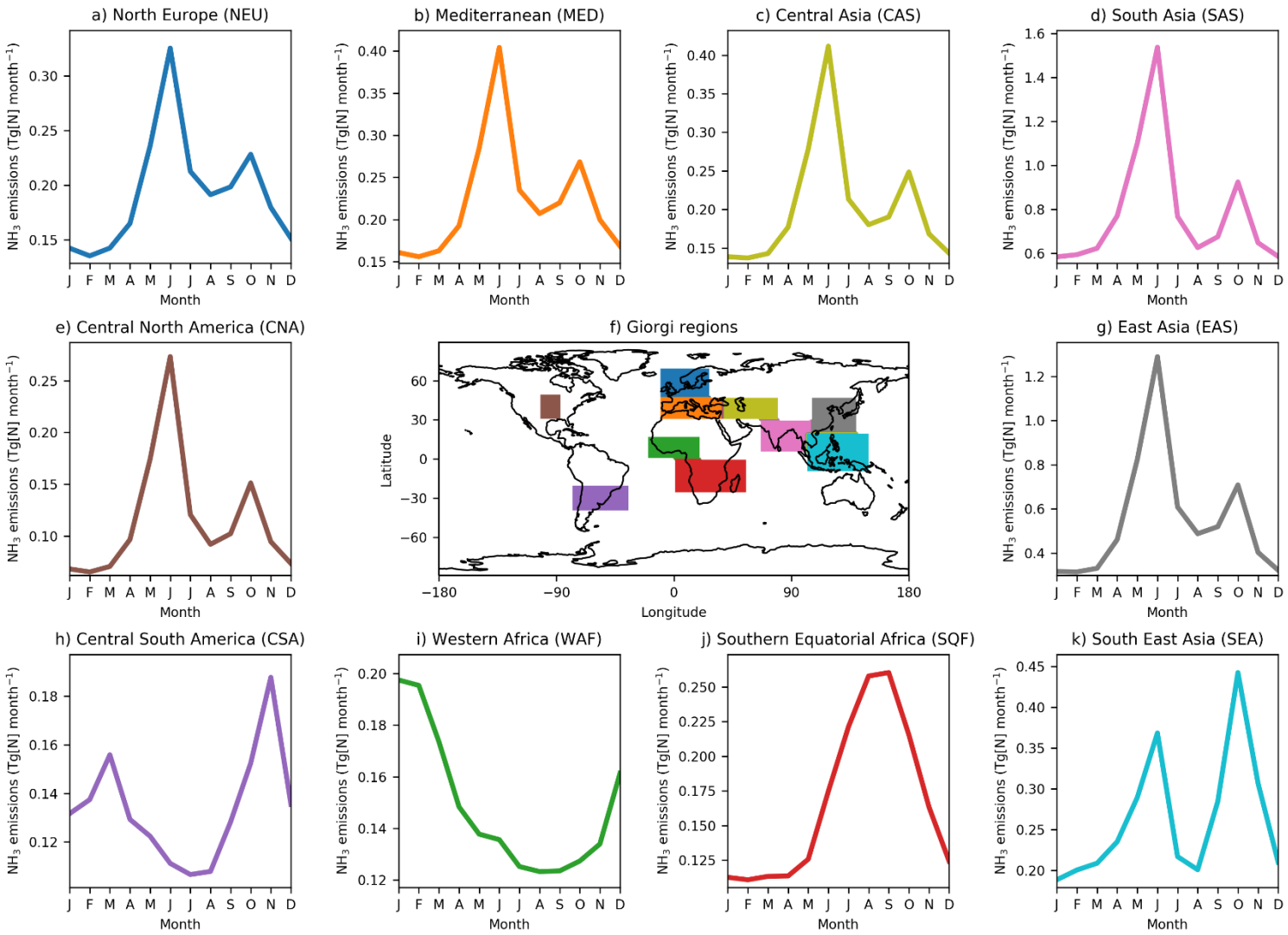

Figure S7: Regional and monthly-mean surface NH_3 emissions time-series for 10 'Giorgi regions' (Giorgi, 2006)

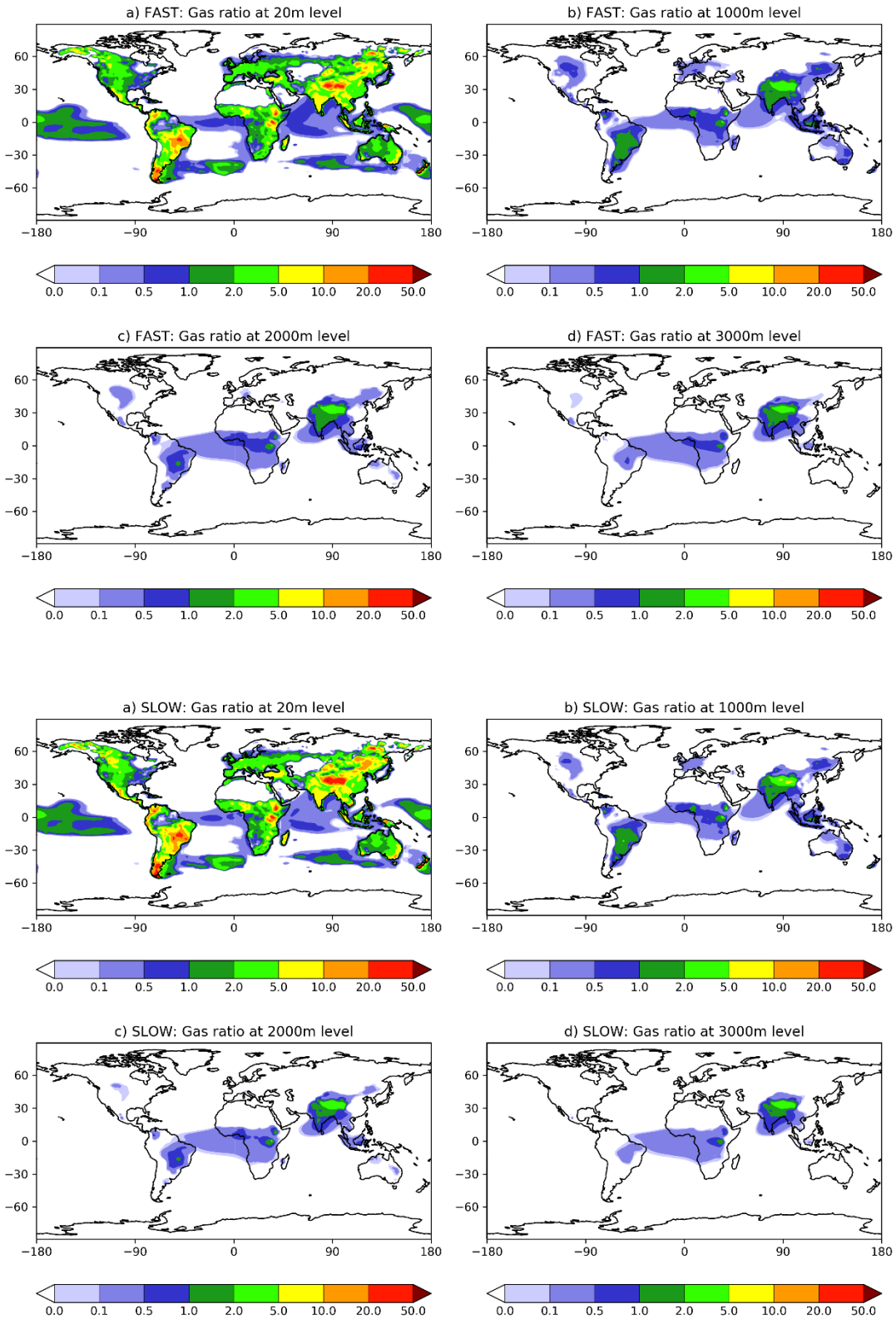

Figure S8: Annual-mean gas ratio in FAST (above) and SLOW (below), defined as $([NH_3] + [NH_4] - 2 \times [SO_4])$ divided by $([HNO_3] + [NO_3])$. Values greater than 1 indicate that ammonium nitrate production is HNO_3 limiting, while values below 1 indicate that production is NH_3 limiting

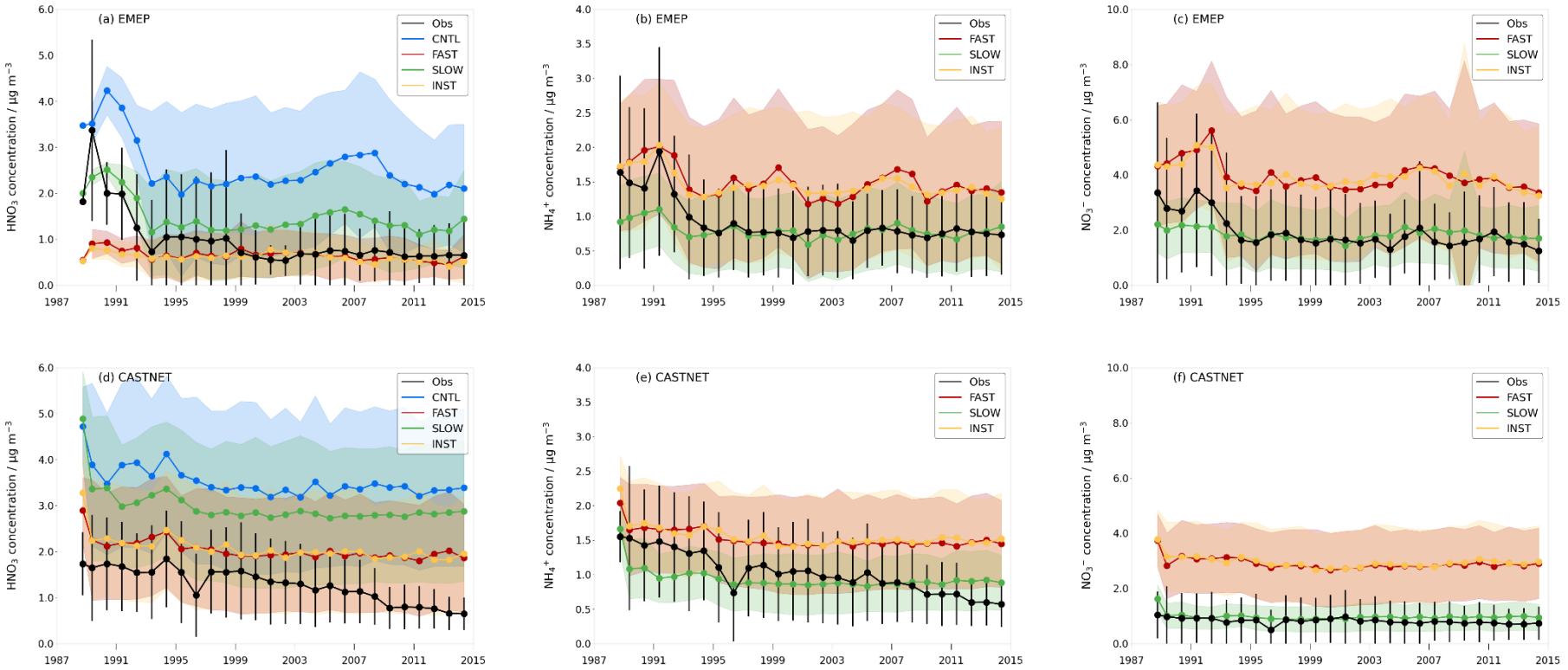

Figure S9: Annual-mean HNO_3, NH_4 and NO_3 concentrations interpolated to CASTNET (US) and EMEP (Europe) observation sites for the period 1994-2013 and averaged over each network. For CASTNET there are a total of 16 Western sites and 33 Eastern sites (49 in total). For the EMEP sites there were 59 for HNO_3, 59 for NH_4 and 80 for NO_3. Note that the years in the MetUM simulations (CNTL, FAST, SLOW, and INST or INSTANT) are arbitrary – the simulations use perpetual year-2000 conditions – and thus the simulations should not be compared with observations on a year-by-year basis.

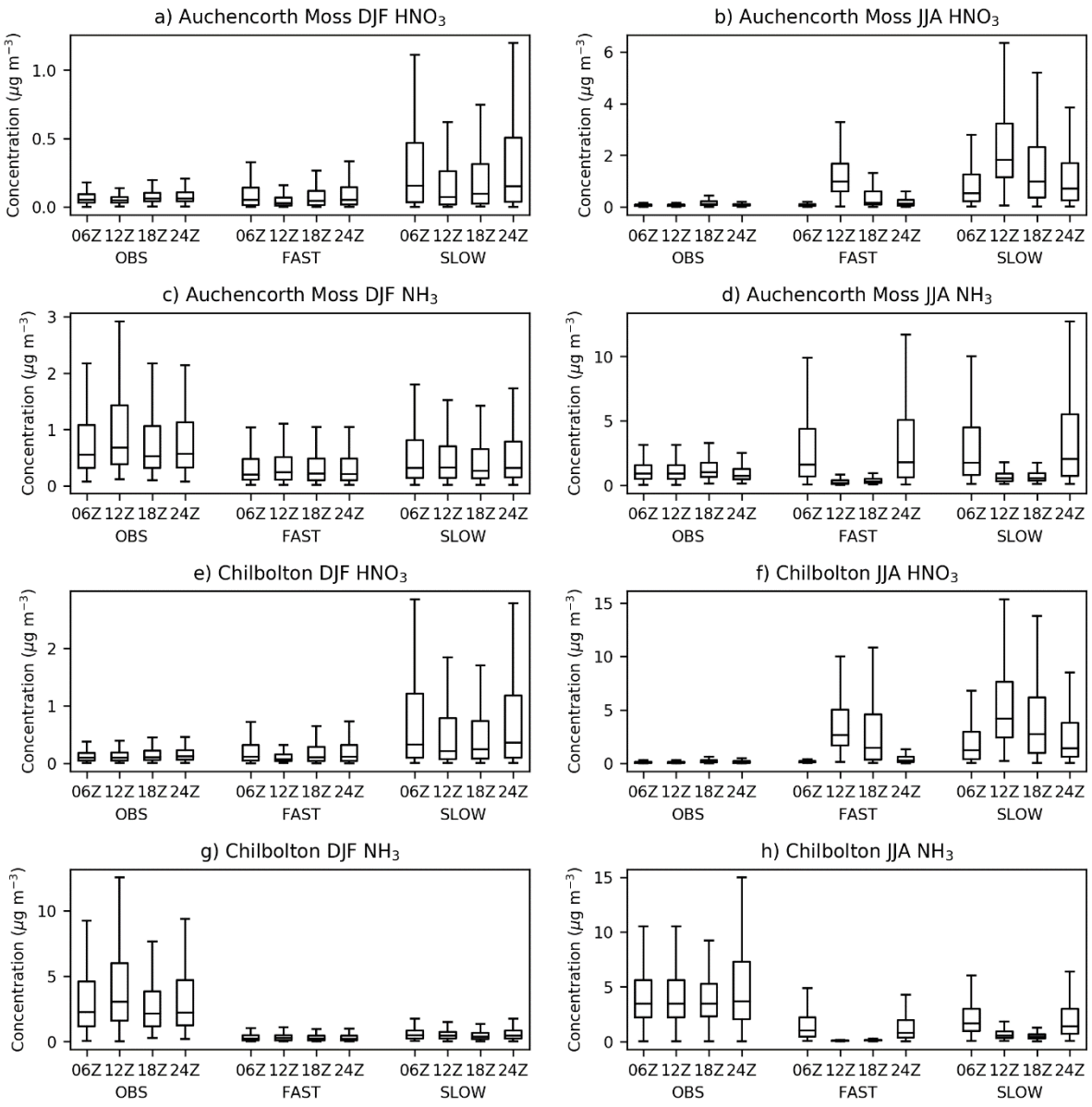

Figure S10: December-February (DJF) and June-August (JJA) diurnal cycles of near-surface HNO_3 and NH_3 concentrations in the FAST and SLOW simulations interpolated to two European Monitoring and Evaluation Programme (EMEP) supersites in the UK – Auchencorth Moss [55.79216ºN, -3.2429ºE] and Chilbolton [51.149617ºN, -1.438228ºE], alongside 6 hourly observations from 2014-2015 for Auchencorth Moss and 2016-2020 for Chilbolton. Equivalent to Fig. 9 in the manuscript.

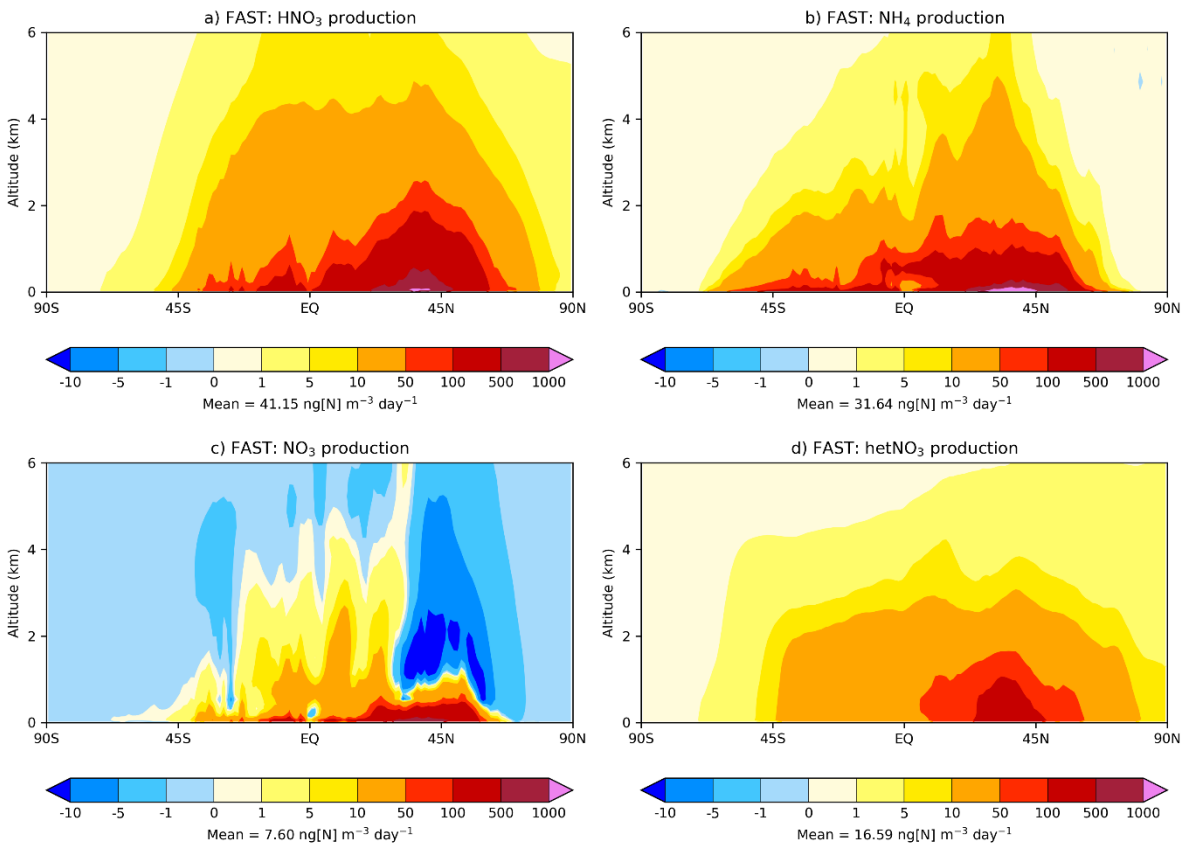

Figure S11: Annual and zonal-mean net HNO_3, NH_4, NO_3, and hetNO_3 production rates in the FAST simulation

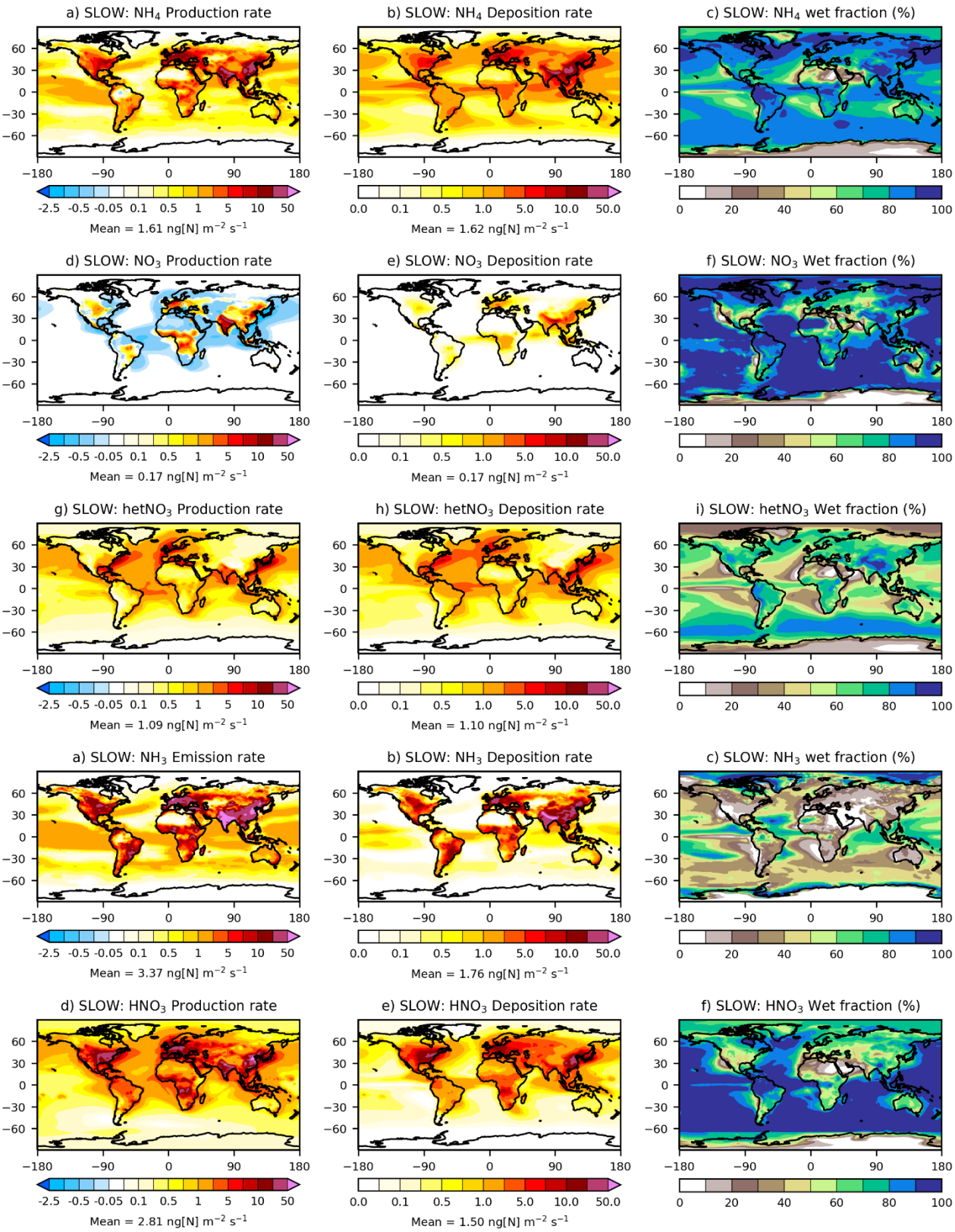

Figure S12: Annual-mean and column-integrated net-production and total deposition rates for NH_4, NO_3, $hetNO_3$, NH_3 and HNO_3, alongside the 'wet fraction' (the ratio of wet scavenging to total deposition) in the SLOW simulation. Equivalent to Fig. 10 in the manuscript